

1 **Zeb1 controls neuron differentiation and germinal zone exit by a mesenchymal-**
2 **epithelial-like transition**

3
4 Shalini Singh¹, Danielle Howell¹, Niraj Trivedi¹, Ketty Kessler², Taren Ong¹,
5 Pedro Rosmaninho³, Alexandre A.S.F. Raposo³, Giles Robinson⁴, Martine F. Roussel⁵,
6 Diogo S. Castro^{3*} and David J. Solecki^{1*}

7
8 1-Department of Developmental Neurobiology, St. Jude Children's Research Hospital,
9 Memphis, TN, USA

10 2-Universite Denis Diderot (Paris VII), Paris, France
11 Current address: Laboratory of Vascular Translational Science, University College
12 London, London, United Kingdom

13 3-Molecular Neurobiology, Instituto Gulbenkian de Ciência Oeiras, Portugal

14 4-Department of Oncology, St. Jude Children's Research Hospital, Memphis, TN, USA

15 5-Department of Tumor Cell Biology, St. Jude Children's Research Hospital, Memphis,
16 TN, USA

17
18 *Correspondence:

20 David J. Solecki, Ph.D.
21 Email: david.solecki@stjude.org

23 Diogo Castro, Ph.D.
24 Email: dscastro@igc.gulbenkian.pt

29 **Short title:** GNP differentiation parallels a MET

30

31

32

33

34 **Abstract**

35 In the developing mammalian brain, differentiating neurons mature morphologically via
36 neuronal polarity programs. Despite discovery of polarity pathways acting concurrently
37 with differentiation, it's unclear how neurons traverse complex polarity transitions or how
38 neuronal progenitors delay polarization during development. We report that zinc finger
39 and homeobox transcription factor-1 (Zeb1), a master regulator of epithelial polarity,
40 controls neuronal differentiation by transcriptionally repressing polarity genes in
41 neuronal progenitors. Necessity-sufficiency testing and functional target screening in
42 cerebellar granule neuron progenitors (GNPs) reveal that Zeb1 inhibits polarization and
43 retains progenitors in their germinal zone (GZ). Zeb1 expression is elevated in the Sonic
44 Hedgehog (SHH) medulloblastoma subgroup originating from GNPs with persistent
45 SHH activation. Restored polarity signaling promotes differentiation and rescues GZ
46 exit, suggesting a model for future differentiative therapies. These results reveal
47 unexpected parallels between neuronal differentiation and mesenchymal-to-epithelial
48 transition and suggest that active polarity inhibition contributes to altered GZ exit in
49 pediatric brain cancers.

50

51 **INTRODUCTION**

52 Construction of the central nervous system's circuitry requires that newborn
53 neurons exit their germinal zone, elaborate axons and dendrites, migrate to a final
54 position and synaptically engage other neurons. Emerging evidence suggests that
55 classic cell polarity signaling molecules, including the Numb endocytic adaptor, the
56 Partitioning defective (PAR) polarity complex and LKB1/SAD kinases, create the cellular
57 asymmetry required for neuronal development and circuit assembly(1-12). Indeed,
58 defective neuronal polarization is proposed to underlie the pathology of some
59 neurodevelopmental or neurodegenerative diseases, and restored polarity has been
60 suggested as a potential therapeutic approach for syndromes involving perturbed
61 polarity-linked mechanisms (13).

62 Given the importance of polarity for neuronal maturation events, great efforts
63 have been made to define mechanisms that cell-extrinsically or -intrinsically control
64 polarity during neuronal differentiation. Most current models suggest the activation of
65 signaling cascades(14-16), transcriptional networks(17), or chromatin states(18, 19)
66 promotes or maintains cell polarity in differentiated neurons. However, it remains
67 unclear how developing neurons undergo discrete transitions during which polarity is
68 delayed or promoted (20, 21). As an example, maturing cortical neurons undergo
69 enhanced polarization via a multipolar to bipolar transition, while GNPs remain
70 unpolarized for an extended period while their progenitor pool expands during cerebellar
71 development.

72 We discovered that the transcription factor Zeb1, a critical regulator of epithelial
73 polarity(22), is highly expressed in unpolarized cerebellar granule neuron progenitors

74 (GNPs) and that its expression diminishes as these cells become polarized cerebellar
75 granule neurons (CGNs). Developing CGNs provide an excellent model of the
76 mechanisms regulating neurogenesis, neuronal differentiation, polarization linked to
77 morphological maturation, and GZ exit(23, 24). They also provide a model of migration
78 mechanisms, since they undergo two migration phases: morphologically unpolarized
79 GNPs and newly postmitotic CGNs migrate tangentially near the cerebellar surface in
80 the external granule layer (EGL) while polarized CGNs migrate radially away from their
81 GZ and cross the molecular layer (ML) to reside within the internal granule layer (IGL)
82 (25-27). In cerebellar medulloblastoma (MB), excessive or constitutive mitogenic
83 signaling in GNPs disrupts the intricate balance of GZ exit and radial migration via
84 unknown motility mechanisms(28-31).

85 Zeb1 functions in many organ systems, including muscle, lymphocytes, and
86 nervous system(32, 33). Proliferating progenitors express Zeb1 in GZs in the
87 developing mouse brain(34). While loss of Zeb1 function in the developing neocortex
88 reduces proliferation in the VZ and SVZ(33), it remains unknown how Zeb1 regulates
89 neural progenitor populations. Studies examining Zeb1 regulation of epithelial cell
90 polarity provide insights. Zeb1 activates stemness pathways in immature, unpolarized
91 epithelial cells and their transformed counterparts(35). It also controls transitions in
92 epithelial differentiation and polarity plasticity: high Zeb1 expression inhibits epithelial
93 differentiation and drives cells toward epithelial-to-mesenchymal transition (EMT), while
94 low expression allows mesenchymal-to-epithelial transition (MET). During EMT, Zeb1
95 acts as a transcriptional repressor that silences adherens junction (AJ) and apical-basal
96 polarity genes(36). Thus, Zeb1 simultaneously blocks differentiation, apical-basal

97 polarity, and junction formation of epithelial cells, locking them into the mesenchymal
98 state.

99 In the developing nervous system, EMT-like events have been observed in the
100 transition of polarized radial glia to their delaminating progeny(37, 38). Given that
101 neuronal progeny undergo multiple polarity transitions after delamination from a radial
102 glial cell, it is open to question how polarity is re-acquired after delamination as nascent
103 neurons mature(20, 21, 39). Do nascent neurons that undergo an EMT-like process
104 also then transition through an MET-like process, like epithelial cells?

105 We have known for more than a decade that persistent SHH signaling blocks GZ
106 exit, but the mechanism has remained a mystery. Here we hypothesized that MET-like
107 events control the onset of neuronal differentiation and GZ exit, which involve cell
108 polarity and cell-cell adhesion transitions. By using gain- and loss-of-function
109 approaches, we found that Zeb1 is necessary and sufficient to maintain GNPs in an
110 undifferentiated, unpolarized, transiently amplifying state within the external germinal
111 layer (EGL) and to control the onset of their GZ exit. Zeb1 represses transcription of
112 polarity and cell adhesion genes, such as *Pard6a*, *Pard3a* and *close homolog of L1*
113 (*Chl1*). By using a functional screen, we found that restored expression of these genes
114 rescues GNP differentiation, neurite extension, and GZ exit. Finally, we examined the
115 link between morphogens and Zeb1 in controlling this process. We found that Sonic
116 hedgehog (SHH), a potent GNP mitogen, maintains Zeb1 expression. Moreover, Zeb1
117 expression persists in MB tumor cells, the transformed GNP counterpart in which SHH
118 signaling is persistently activated. Zeb1 loss-of-function or restored Zeb1 target
119 expression rescued the GZ exit phenotype in *Patched1* (*Ptch1*)-deficient GNPs, the

120 progenitors of SHH-subgroup MB. Our findings show that CGN differentiation bears a
121 remarkable similarity to mesenchymal-to-epithelial transition. The balance of EMT-like
122 vs. MET-like processes and of proliferative vs. maturation processes may be a key
123 developmental mechanism that, when disrupted, contributes to the pathological
124 alteration of GZ exit in neurodevelopmental disorders and pediatric cancers.

125

126 RESULTS

127 **Zeb1 is expressed in GNPs and is extinguished during CGN differentiation.** To test
128 the hypothesis that MET-like events control the onset of GNP differentiation and GZ
129 exit, we first surveyed expression of the canonical EMT regulators Snail1, Snail2, Twist,
130 and Zeb1 in GNPs. Quantitative RT-PCR revealed that Zeb1 is the primary EMT factor
131 expressed in GNPs during the early postnatal (P) peak of neurogenesis, and that
132 expression diminishes as GNPs exit the cell cycle to differentiate into CGNs: at P7
133 Zeb1 mRNA was 28-fold higher than the next most abundant transcription factor, *Snail1*
134 (Figure 1a). Zeb1 protein expression confirmed our RNA analysis where it is expressed
135 primarily in the EGL at P7 and greatly reduced at P15 (Figure 1b). At P7, Zeb1 is co-
136 expressed with the proliferation marker Ki67 and two markers of GNP identity Siah2,
137 and Meis1/2, and is greatly reduced in cyclin-dependent kinase inhibitory protein
138 p27^{Kip1}/Cdkn1b (referred as p27 thereafter)-positive postmitotic CGNs in the inner EGL.
139 We noted a subpopulation of Zeb1 positive cells in deeper layers of the cerebellum at
140 P7. These cells represent a mixture of white mater interneuron or oligodendrocyte
141 precursors as these cells also express Pax2(40) or Olig2(41) (Figure1-figure
142 supplement 1). In GNPs, Zeb1 mRNA expression was inversely correlated with the

143 expression of the apical-basal polarity genes *Pard6a* and *Prkcz* (Figure 1c). Not only did
144 *Pard6a* mRNA increase as CGN differentiation proceeded, but the promoter of this gene
145 was active in individual GNPs at the border of the GZ, prior to their entry into the inner
146 EGL (Figure 1d). Taken together, these results indicate that GNPs are mesenchymal-
147 like, as they express a high level of Zeb1 and low levels of polarity genes.

148 **Zeb1 gain- or loss-of-function regulates CGN differentiation, neurite extension,
149 and GZ exit.** Given the Zeb1 expression profile, we reasoned that this transcription
150 factor might regulate GNP differentiation. We used a gain-of-function approach to
151 examine Zeb1's role in this process, as this method maintained Zeb1 expression in
152 GNPs and because diminished Zeb1 expression coincides with differentiation to CGNs.
153 Purified P7 GNPs were nucleofected with an expression vector that encodes mouse
154 Zeb1. After 1 day *in vitro*, control GNPs displayed features of differentiated CGNs: they
155 extended neurites, expressed p27 and no longer expressed Ki67 and Atoh1, a marker
156 of proliferating GNPs (Figure 2a, b) (31, 42). In contrast, Zeb1-expressing cells had
157 short, multipolar extensions (\bar{x} length=140 ± 13 µm vs 60 ± 3 µm), expressed reduced
158 p27 and sustained levels of Ki67 and Atoh1, indicating arrested maturation and
159 proliferating, GNP-like state. While Zeb1-expressing GNPs were motile on time-lapse
160 microscopy in dissociated cultures, they did not display the typical two-stroke
161 nucleokinesis cycle used by differentiated CGNs and had an apolar, isotropic f-actin
162 distribution reminiscent of GNP morphology *in vivo* (Videos 1 and 2). At the moment, it's
163 unclear whether this mesenchymal-like morphology and random migration direction is
164 due to a disturbed intrinsic polarity program or perturbed glial binding.

165 We next assessed the effect of Zeb1 function on GNP differentiation, GZ exit and
166 migration to the IGL with the *ex vivo* cerebellar slice assay developed in our laboratory
167 that specifically label GNPs¹² (Figure 2c and d, see Figure 20-figure supplement 1 for
168 detailed analysis). We used two independent shRNA vectors to silence *Zeb1* in P7 EGL
169 (see Figure 2-figure supplements 1 and 2 for second shRNA migration data and
170 validation). After 24 h *ex vivo*, control EGL cells resided in the GZ and incorporated
171 EdU, not having differentiated into CGNs or begun migrating to the IGL. In contrast,
172 *Zeb1* silencing increased migration toward the IGL (\bar{x} distance=34 ± 10µm vs 68 ± 18
173 µm) and reduced EdU incorporation (22.6 ± 1.0% vs 7.6 ± 1.8% EdU positive), showing
174 that *Zeb1* loss-of-function promotes differentiation and migration toward the IGL. We
175 next confirmed that *Zeb1* activity inhibited GZ exit, using a gain-of-function approach.
176 P7 EGL was electroporated with an expression vector for *Zeb1*. After 2 days *ex vivo*,
177 control CGNs entered the molecular layer and IGL, while *Zeb1*-expressing CGNs
178 remained within the EGL (\bar{x} distance=75 ± 3 µm vs 40 ± 6 µm, Figure 2d) and continued
179 to incorporate EdU (3.3 ± 0.4% vs 10.9 ± 0.1% EdU positive). To further examine the
180 role of *Zeb1* in GNP differentiation *in vivo* we scored Tag1 and NeuN expression in the
181 EGL of E18.5 *Zeb1* null embryos (a time-point prior perinatal lethality observed in *Zeb1*
182 null embryos). Consistent with our *ex vivo* gene silencing results, loss of *Zeb1* function
183 *in vivo* leads to an increase in Tag1 and NeuN differentiation marker gene expression,
184 indicating an increase of neuronal differentiation in the absence of *Zeb1* (Figure 2e).
185 These observations indicate that *Zeb1* inhibits differentiation of GNPs to CGNs and is
186 necessary and sufficient to restrict GNPs to their GZ niche. They also suggest that *Zeb1*

187 inhibits GNP polarization, as neurite extension, two-stroke nucleokinesis and GZ exit
188 depend on polarity signaling complexes in CGNs.

189 **Zeb1 transcriptionally represses genes associated with neuronal maturation, cell**
190 **polarity and cell adhesion.** Having learned that Zeb1 inhibits GNP differentiation and
191 potentially the downstream events associated with CGN polarization, we next sought to
192 identify Zeb1 targets to determine how sustained Zeb1 expression maintains GNPs. We
193 reasoned that as Zeb1 gain-of-function strongly inhibits GNP differentiation, it would
194 provide a basis to identify potential Zeb1 targets. We prepared RNA from P0, P7 and
195 P15 GNPs and used Affymetrix DNA arrays to compare their transcriptomes of these
196 cells with those of pure, FACS-sorted GNP populations nucleofected with control, Zeb1-
197 or HES1 expression vectors (Figure 3a, ArrayExpress accession number: E-MTAB-
198 3557). We included the transcription factor HES1 because it is a known repressor of
199 GNP differentiation downstream of the Notch2 receptor(43). GNPs were selected for
200 our developmental expression analyses as it is well established this transiently
201 amplifying progenitor population expresses early CGN differentiation markers; such as
202 TAG1, L1, NRCAM, NeuroD1 or TIS21 prior to their final cell cycle (44-46). Zeb1 gain-
203 of-function suppressed a group of genes increasingly expressed between P0 and P15
204 (Figure 3b, Figure 3-figure supplement 1), consistent with previous observations that
205 Zeb1 acts as a transcriptional repressor. Gene ontology analysis revealed this group of
206 genes to be associated with tissue morphogenesis, epithelial polarization, cell adhesion
207 and control of cell motility. Key members of the apical or basolateral polarity pathways
208 (*Pard6a* *Pard3a*, *Dlg2* and *Lin7a*) and *Cdh1* AJ adhesion molecule were among the
209 Zeb1-repressed genes. In parallel, we analyzed the EMT/MET signature upon Zeb1

210 gain-of-function in GNPs, using a pathway-focused PCR array. Various genes
211 previously shown to be induced during EMT were enriched in these GNPs, while a class
212 of MET-related genes were repressed (see Tables in Supplementary files 1A and 1B).
213 For further validation we selected a group of genes that included polarity complex genes
214 (*Pard6a*, *Pard3a*, *Dlg2* and *Lin7a*), cell adhesion genes (*Cdh1* and *Chl1*), transcription
215 factors associated with cell differentiation (*Bhlhe40* and *Nfib*), and three randomly
216 selected genes (*Sorl1*, *Flt1*, and *Cdk5r1*), most of which were not/are not significantly
217 repressed by HES1. Not only were many of these genes expressed in the normal
218 developmental time course (Figure 3-figure supplement 2) and validated as suppressed
219 in Zeb1-expressing GNPs (Figure 3c), the protein expression of many of them was
220 mutually exclusive with Zeb1 or Ki67 (Figure 3d). A previous study in our laboratory
221 demonstrated a similar expression profile for Pard3a (12). These results suggest that
222 many of the putative targets identified are bona fide CGN differentiation markers were
223 expressed at low levels in early postnatal GNPs. Increased polarity gene expression in
224 differentiated CGNs, their mutually exclusive expression with GNP markers, and their
225 suppression by Zeb1, further suggest a parallel between GNP differentiation and MET.

226 We next sought to investigate whether Zeb1 directly regulates genes differentially
227 expressed in our array. As a prelude, we first assessed global Zeb1 binding sites in a
228 ChIP-seq data set from NS5 mouse neural stem cells, which, like GNPs, express high
229 levels of Zeb1 (Figure 4-figure supplement 1, ArrayExpress accession number: E-
230 MTAB-3560). Many of the proximal promoters of key apical-basal polarity genes
231 (*Pard6a*, *Pard6b*, *Pard3a*, *Pard6g*) and other Zeb1-regulated genes identified in our
232 screen (*Chl1*, *Limk2*) showed clear Zeb1 binding peaks, suggesting that they are direct

233 targets (Figure 4-figure supplement 2). Computational analyses comparing the genome-
234 wide Zeb1 binding profile to the Zeb1-regulated genes identified by expression profiling
235 showed Zeb1 binding events are highly associated with downregulated genes (Figure
236 4a-c), further pointing to Zeb1 as a transcriptional repressor in neural stem/progenitor
237 cells. We next validated Zeb1 binding to key genes in purified P7 GNPs by ChIP PCR
238 (Fig 4d). No binding was detected at non-functional regions of the genome in the
239 *androgen receptor* and *GAPDH* genes. Weak but consistent binding was detected in the
240 proximal upstream regions of *Limk2* and *Lin7a*. Strong Zeb1 binding was observed at
241 positive control regions in the *Zeb1* gene and *Cdh1* gene, at the proximal upstream
242 sequences of *Pard6* and *Pard3a* genes and at an intronic site in the *Chl1* gene. Overall,
243 these results indicate that Zeb1 directly regulates genes expected to play a role in cell
244 adhesion and apical-basal polarity.

245 ***Par6a, Pard3a and Chl1 are Zeb1 targets required for CGN differentiation.*** Given
246 the expression profile of Zeb1 targets and the mutually exclusive expression of these
247 genes and *Zeb1*, we postulated that some of these targets may facilitate CGN
248 differentiation, neurite extension and GZ exit downstream of Zeb1. We individually
249 expressed validated targets in the context of our *in vitro* (neurite extension, Ki67 or p27
250 expression status) and *ex vivo* (GZ exit and EdU incorporation status) Zeb1 gain of
251 function assays (Figure 2a, b and d) to determine whether restoring individual target
252 expression would rescue the Zeb1 phenotypes and thus functionally prioritize these
253 targets. For this small functional screen we selected key polarity molecules (*Pard6a*,
254 *Pard3a*, *Lin7a*, *Dlg2*), adhesion receptors (*Cdh1*, *Chl1*, constitutively active JAM-C),
255 genes associated with cell differentiation (*Sorl1*, *Bhlhe40*, *Nfib*) and randomly selected

256 genes (*Flt1* VEGF receptor, *Cdk5r1*). Our laboratory has previously shown that Pard6a
257 and Pard3a are required for CGN migration and GZ exit(2, 12). Chl1 regulates neurite
258 initiation, neuronal migration and neuronal dendrite orientation in the developing
259 neocortex(47, 48). Lin7 and Dlg homologs are components of the apical or basolateral
260 polarity complexes in epithelial cells where Dlg recruits Lin7 to distinct membrane
261 domains(49). Nfib regulates CGN differentiation(50), and Cdk5r1 regulates Cdk5 activity
262 during neuronal migration(51). JAM-C is not a Zeb1 target but was included because
263 reduction off Pard3a activity reduces JAM-C adhesion and this constitutively active
264 receptor complements CGN adhesion in the absence of Pard3a function(12). Prior to
265 the screen, we carefully titrated the quantity of expression vector needed to roughly
266 double each target's expression in control CGNs to complement Zeb1-mediated target
267 repression (data not shown). We observed diversity in the way individual targets
268 modified the Zeb1 gain-of -function phenotypes in *in vitro* and *ex vivo* assays
269 (Supplemental Figure 5 and 6; Figure 6-figure supplement 1, Supplementary file 2).
270 Restored expression of Pard6a, Pard3a, and Chl1 rescued all measured phenotypes to
271 normal levels in CGNs. Individual introduction of each of these downstream Zeb1
272 targets allowed GNPs to acquire mature CGN status, characterize long neurites,
273 expression of the p27 cell cycle inhibitor, absence of Ki67 labeling or EdU incorporation
274 and GZ exit with subsequent migration to the IGL, even with Zeb1 gain-of-function.
275 Constitutively active Jam-C and the basolateral polarity protein Lin7a did not influence
276 maturation parameters *in vitro* (Figure 5); however, both stimulated cell cycle exit, GZ
277 exit and migration *ex vivo* (Figure 6), suggesting that they act non-cell-autonomously in
278 the complex *ex vivo* environment. Dlg2 stimulated cell cycle exit and p27 expression in

279 all conditions tested but was unable to rescue neurite extension or migration *ex vivo*.
280 Four genes, *Sorl1*, *Bhlhe40*, *Nfib*, and *Cdk5r1*, reestablished p27 expression. p27 is
281 known for its cell cycle inhibitory and cytoskeletal regulatory properties; however, p27
282 expression alone in *Sorl1*-, *Bhlhe40*-, *Nfib*- or *Cdk5r1*-expressing cells was insufficient
283 to rescue the other features of mature CGNs, such as neurite extension, loss of Ki67
284 labeling/EdU incorporation, or GZ exit and migration to the IGL. Restored expression of
285 *Nfib* and *Flt1* enhanced neurite extension but failed to rescue the full spectrum of
286 mature CGN features, much like the genes that stimulated p27 expression.
287 Additionally, longer term *ex vivo* incubations revealed that *Cdh1*, *Cdk5r1* and *Sorl1* were
288 not sufficient to rescue IGL-directed migration of Zeb1 over-expressing cells (Figure 6-
289 figure supplement 2). Interestingly, *Bhlhe40* expression, a negative regulator of EMT
290 could rescue with a 72 hour *ex vivo* incubation. Time-lapse imaging revealed of
291 cultured neurons revealed that *Pard6a*-, *Pard3a*-, and *Chl1*-rescue also restored two-
292 stroke nucleokinesis and JAM-C adhesion levels, two cell biological outputs of the PAR
293 complex function in maturing CGNs (2,12) (see Videos 3-12).

294 Given that *Pard6a* and *Chl1* were among the targets whose restoration most
295 potently rescued Zeb1 gain-of-function phenotypes, we sought mechanistic insight into
296 this rescue by further characterizing expression of key factors in proliferating GNPs, D
297 type Cyclins and Atoh1. Restored *Pard6a* and *Chl1* expression did not affect the levels
298 at which Zeb1 suppressed its target genes, indicating that *Pard6a* and *Chl1* did not
299 counteract Zeb1 at the transcriptional level or non-specifically reduce Zeb1 target
300 repression in our assay system (Figure 7a). Moreover in the case of *Chl1* protein,
301 restored *Pard6a* and *Pard3* did not rescue *Chl1* expression as assayed by

302 immunocytochemistry in dissociated CGNs (Figure 7-figure supplement 1). Restored
303 Pard6a or Chl1 expression reduced Zeb1-mediated activation of CyclinD1 and CylinD2
304 mRNA and Atoh1 protein levels, all of which are required to maintain GNPs in the
305 undifferentiated state (Figure 7b and c) (31, 42, 52). The broad rescue of Zeb1 gain-of-
306 function phenotypes by the Pard6a and Pard3a polarity proteins and the Chl1 adhesion
307 molecule demonstrates that these Zeb1-supressed targets are prerequisites for mature
308 CGN characteristics. These findings also reinforce the parallel between CGN
309 differentiation and polarity regulation in cells of epithelial origin. Not only do Zeb1 and
310 polarity proteins show mutually exclusive expression in GNPs and CGNs, but the
311 functional screen also shows that their functional antagonism regulates the balance
312 between the GNP and CGN states.

313 **Zeb1 is regulated by SHH, highly expressed in SHH-subgroup medulloblastoma**
314 **and functionally required to retain Ptch1-deficient GNPs in the GZ.** Having found
315 that Zeb1 controls GNP differentiation and GZ exit by regulating neuronal polarity and
316 adhesion, we next sought to identify factors that can regulate Zeb1 in GNPs. We
317 reasoned that SHH, the required mitogen for GNP proliferation, may regulate Zeb1
318 expression given that it not only stimulates progenitor proliferation but also blocks CGN
319 differentiation(53). GNP cultures treated with SAG, a potent small-molecule SHH
320 agonist, displayed not only elevated Zeb1 but also decreased Pard6a and Chl1 proteins
321 (Figure 8a, b). These results suggest that Zeb1 and some of its targets act downstream
322 of the SHH signaling cascade.

323 The SHH pathway is activated in both mouse and human MBs derived from
324 GNPs(54-57). As SHH activation led to elevated Zeb1 in normal GNPs, we next

325 examined the expression levels of Zeb1 and its targets in a mouse SHH MB model from
326 *Ptch1 +/-, Cdkn2c -/-* mice in which SHH signaling is constitutively activated (58). Unlike
327 normal P15 cerebellum (Figure 1b), MBs from adult *Ptch1+/-, Cdkn2c-/-* mice displayed
328 high levels of Zeb1 expression (Figure 8c). MBs contain subpopulations of cells that
329 can proceed with neuronal differentiation. Zeb1 expression was complementary with
330 that of class III beta-tubulin/Tuj1, an early neuronal differentiation marker, indicating that
331 Zeb1 expression is extinguished in both normal and tumor-derived cells proceeding
332 toward the differentiated phenotype. We also quantified the RNA expression of Zeb1
333 and its targets by qRT-PCR in normal GNPs and in mouse SHH MBs. Mouse MBs
334 contained higher levels of *Zeb1* RNA than GNPs purified at P7, the time of peak Zeb1
335 expression (Figure 8d). Moreover, most Zeb1 targets identified in our Affymetrix Gene
336 Chip array were expressed at lower levels in mouse MBs than in P7 GNPs, with the
337 sole exception of *Pard3a* (Figure 8d). To broaden our analysis outside of mouse MB, we
338 quantified *ZEB1* RNA in human MB samples(56). *ZEB1* RNA was about four times
339 higher in the human SHH MB subgroup compared to WNT, Group3 and Group4 MBs
340 (Figure 8e). These results indicate that in mouse and human MB, Zeb1 expression is
341 elevated when the SHH pathway is activated, supporting the link we observed between
342 SHH and Zeb1 in normal GNPs. Elevated Zeb1 expression paralleled reduced
343 expression of the targets identified in our Zeb1 gain-of-function expression profiling,
344 validating our findings in primary GNPs.

345 Pre-neoplastic GNPs show a greatly delayed GZ exit, the first overt phenotype
346 observed in mouse MB models with chronic SHH activation (*Ptch1+/- ; Ptch1+/-,*
347 *Cdkn2c-/- ; and Ptch1Floxed mice*)(28, 30, 58). While there is a firm link between

348 proliferation and delayed differentiation in pre-neoplastic GNPs, it is unknown how
349 deregulated SHH signaling delays GZ exit. Given that Zeb1 controls GNP differentiation
350 and GZ exit and that its expression is linked with elevated SHH signaling, we postulated
351 that Zeb1 function, and its transcriptional repression of polarity genes, may be related to
352 the GZ exit phenotypes of GNPs with an activated SHH pathway. We developed an ex
353 vivo model to examine the GZ exit status of GNPs exposed to chronic SHH stimulation:
354 we electroporated vectors encoding codon-optimized Cre recombinase or its inactive
355 mutant into P7 cerebellar EGL from mice homozygous for *Ptch1* harboring loxP sites
356 flanking exons 8-9 (*Ptch1*^{flox/flox} mice)(59). As the *Ptch1* receptor is a negative regulator
357 of SHH signaling, conditional *Ptch1* deletion leads to potent constitutive activation of the
358 pathway and, over a longer time, GNP malignant transformation. GNPs expressing Cre
359 recombinase remained largely within the EGL, but migration was unaltered by a
360 catalytically inactive mutant (\bar{x} distance=41.4 ± 5.8 μm vs. 71.1 ± 7.8 μm; Figure 8f,
361 Figure 8-figure supplement 1). To examine Zeb1 and Zeb1-target function in the GZ exit
362 phenotype of *Ptch1*-deficient GNPs, we co-electroporated P7 EGL from *Ptch1*^{flox/flox}
363 mice with Cre recombinase and an shRNA silencing Zeb1 or vectors encoding Pard6a,
364 Chl1 and Lin7a, which were expressed at low levels in the mouse Zeb1-expressing MB
365 cells. Zeb1 silencing or increased Pard6a, Chl1 and Lin7a expression restored GZ exit
366 and migration to the IGL to near wild-type levels. Taken together, these results show
367 that Zeb1 is functionally required downstream of SHH signaling to control GZ exit.
368 Moreover, the MET-like transition that occurs in CGN differentiation is evident not only
369 during normal development but also in an ex vivo model of pathological GZ exit
370 implicated in cerebellar tumorigenesis.

371

372 **DISCUSSION**

373 Here we identified a key developmental mechanism of the mammalian brain wherein
374 the onset of neuronal polarization and differentiation is restrained by Zeb1-mediated
375 active inhibition of polarity in neuronal progenitors. Conversely, diminished repression of
376 polarity genes or adhesion receptors accompanying Zeb1 downregulation promotes
377 morphological maturation, GZ exit, and IGL-directed migration of CGNs in the
378 developing cerebellum. We found that the Zeb1 EMT inhibitor is downregulated as
379 GNPs begin to exit the EGL niche and that Zeb1 loss-of-function spurs precocious GZ
380 exit and withdrawal of GNPs from the cell cycle. Failure to downregulate Zeb1 delays
381 the onset of key polarity gene or adhesion receptor expression, morphological
382 maturation, GZ exit, and migration to the IGL. Restoration of Pard6a, Pard3a and Chl1
383 expression alone is sufficient to rescue the CGN fate in the context of Zeb1 gain-of-
384 function. These findings show that polarization is not only triggered by differentiation
385 programs in newborn neurons but is also obstructed in transiently amplifying progenitor
386 cells, much as polarity is regulated in epithelial-mesenchymal and mesenchymal-
387 epithelial transitions (see Figure 9).

388 **MET and neuronal differentiation**

389 Throughout the developing brain, newborn neurons are similarly challenged to
390 depart their GZ niche and integrate into a functional circuit (25, 60), and at each stage
391 of their differentiation these cells must undergo reorganization of their polarity (17, 39).
392 While radial glial cells, migrating neurons and neurons elaborating axons or dendrites
393 display a polarized morphology, transiently amplifying progenitors and newly

394 delaminated neurons are temporarily less polarized. Conceptual parallels have been
395 made between epithelial and neuronal polarity (61). Recently, Foxp- or Scratch-
396 mediated inhibition of classical cadherins was recently shown to spur neuronal AJ loss,
397 transition away from radial glial polarity, and delamination from the VZs of the spinal
398 cord and cortex(37, 38). The parallel between Foxp- and Scratch-mediated
399 delamination of neurons and EMTs in epithelial cells is incomplete, as both delamination
400 events may occur in postmitotic neuronal progeny. Also, we still have no clear idea how
401 immature neurons or their progenitors transition out of their low polarity states during
402 terminal differentiation. Our work demonstrates that transiently amplifying cerebellar
403 progenitors display mesenchymal characteristics, expressing high levels of Zeb1 and
404 low levels of polarity proteins and adhesion molecules needed for maturation to CGNs.

405 How similar are CGN differentiation and MET? As illustrated in our model (Figure
406 9), METs are associated with acquisition of a mature, polarized morphology. Zeb1 locks
407 GNPs into a very immature morphology, just as it blocks apical-basal polarization in
408 epithelia. Second, a common MET pattern is extensive migration followed by a final
409 integrative positioning event(62). At the population level, GNPs migrate to cover the
410 cerebellar anlage, migrate within the EGL, and finally undergo differentiative migration
411 to the IGL. Our results show that Zeb1 is necessary and sufficient to confine GNPs to
412 their GZ niche, where migration is restricted to the cerebellar surface. Finally, METs
413 involve a changing balance of cell-matrix and cell-cell contacts, in which mesenchymal
414 cells engage in extracellular matrix adhesions and differentiated epithelial cells engage
415 in cell-cell adhesions(63). Similarly, early electron microscopy studies showed that
416 GNPs remain largely contiguous with the matrix-rich pial basal lamina until they

417 differentiate(64) and develop extensive cell-cell contacts (65, 66). Interestingly, we
418 found that promotion of cell-cell contact with constitutively active JAM-C and restored
419 Chl-1 expression rescues Zeb1 gain-of-function phenotypes. One key difference
420 between GNP differentiation and epithelial polarity is the mir200 class of micro RNAs
421 that inhibits Zeb1 expression in epithelial cells are not expressed in CGNs(67). Overall,
422 CGN differentiation, which is accompanied by downregulation of Zeb1, enhanced Zeb1
423 target expression, morphological maturation and GZ exit, bears remarkable similarity to
424 the METs of epithelial cells as they incorporate into epithelial tissues. At the moment, it
425 is unclear if additional EMT regulatory transcription factors behave similarly in GNP
426 differentiation. While Zeb1 was clearly the highest expressed EMT regulatory factor
427 relative to 18S RNA, necessity and sufficiency testing was not performed on low
428 abundance genes like *Sna1* or *Sna12*.

429 We anticipate that MET associated with Zeb1 downregulation is also relevant to
430 other brain regions. Both GNPs and cortical intermediate progenitors have delaminated
431 from a parental radial glia, amplify transiently in a displaced GZ (EGL vs SVZ), express
432 some similar markers (Tbr2, Id proteins, Tis21, Zeb1), and assume a simple
433 morphologic form before differentiation. Our ChIP-seq studies show that Zeb1 occupies
434 the promoters of polarity genes in mouse neural stem cells with telencephalic features,
435 raising the possibility that Zeb1 may regulate the polarity of telencephalon cells. We
436 observed that Zeb1 inhibits GNP expression of the GTPases Rnd1 and Rnd3 (data not
437 shown), which promote VZ delamination, inhibit intermediate progenitor proliferation and
438 enhance multipolar to bipolar transition in the neocortex, much as Zeb1 targets function
439 in GNPs(68, 69).

440 **Zeb1 and neuronal polarity**

441 Neuronal polarity regulation by Zeb1 differs from the mechanisms described in forebrain
442 and cerebellar neurons. Neuronal polarization in the hippocampus and cortex depends
443 on the balance of cues and signaling from extracellular, intracellular and cytoskeletal
444 sources that shape forming axons or dendrites(15). Transcriptional control mechanisms
445 involving FOXO, SnoN1/2, NeuroD1 and NeuroD2 have been found to promote discrete
446 stages of morphological CGN maturation, illustrating the partial dependence of axon-
447 dendrite morphogenesis on competence that develops during differentiation(17). Our
448 findings show a new level of regulation of the onset of neuronal polarity in which active
449 gene expression programs in neuronal progenitors cells can delay their competence to
450 polarize. Thus, transiently amplifying progenitors are unpolarized not only because they
451 do not yet express intrinsic maturation components but also because they express
452 factors, like Zeb1, that restrain their polarization.

453 **Zeb1 and aberrant germinal zone exit**

454 CGNs offer not only a model of neural development but also an excellent system
455 to study the dysregulation of signaling pathways in disease. The best example is the link
456 between SHH signaling, GNP proliferation, and MB tumorigenesis. Humans with
457 activating mutations in the SHH pathway are genetically predisposed to MBs that bear
458 many similarities to GNPs(70-72). Available mouse models can recapitulate SHH-
459 associated MB(28, 30, 58). During cerebellar development, GNPs stream from the
460 rhombic lip to cover the cerebellar anlage, expand clonally in the EGL in response to
461 Purkinje cell-derived SHH, then exit mitosis and their GZ niche and migrate inward to
462 the IGL(73). When the SHH signaling pathway is deregulated *in vivo*, cohorts of GNPs

463 fail to exit their GZ niche and continue to proliferate on the cerebellar surface well past
464 the normal interval(28). Although migration from the mitotic niche is proposed to be
465 linked to GNP cell cycle exit(74), the specific downstream GZ exit or migration
466 mechanisms are unknown. Our finding that SHH maintains Zeb1 expression and that
467 Zeb1 target expression is reduced in MB reveals an antagonism between the main GNP
468 mitogen and the polarity required for GZ exit. This antagonism suggests that SHH
469 inhibits the MET-like event we showed to control GNP GZ exit and that pre-neoplastic
470 GNPs or MB cells are inherently polarity-deficient. The possibility that Zeb1 controls an
471 active program to block polarization is particularly relevant to MB. These tumor cells
472 express high levels of the FOXO and NeuroD transcription factors that promote CGN
473 polarization, but they are insufficient to induce polarization of transformed GNPs. Thus,
474 Zeb1 is a candidate factor that may act downstream of SHH in MB to counteract the
475 polarization program. Finally, our results suggest future studies to determine whether
476 restoring the polarity balance in MB will yield therapeutic benefit as a complement to
477 existing first line- or targeted therapies.

478 In *Ptch1*-deficient, Zeb1-overexpressing GNPs, restored expression of selected
479 Zeb1 targets rescues CGN differentiation, GZ exit and migration to the IGL. How do the
480 targets, such as the PAR complex and Chl1, promote these events? In the context of
481 Zeb1 gain-of-function, Pard6a and Chl1 expression reduced Zeb1 activation of
482 CyclinD1, CyclinD2, and Atoh1, each of which is essential to maintain GNP proliferation
483 (31, 42, 52). Thus, Pard6a and Chl1 appear to cell-intrinsically promote CGN
484 differentiation. Consistent with this hypothesis, Pard6a and Chl1 gain-of-function in
485 normal GNPs spurs precocious germinal zone exit (data not shown). In preliminary

486 time-lapse imaging studies, Pard6a, Pard3a and Chl1 also rescued two-stroke motility
487 and JAM-C adhesion levels (see Videos 3-12). While it is intriguing that PAR complex
488 and Chl1 behave similarly in our functional genomics screen, further studies are
489 necessary to clarify their potential functional interactions. Finally, an additional area of
490 further investigation is the cooperation between transcriptional and post-transcriptional
491 mechanisms for polarity regulation. While Pard3a is clearly transcriptionally repressed
492 by Zeb1, its mRNA does not display the same elevation displayed by other targets after
493 Zeb1 expression diminishes. Interestingly, Pard3a protein expression levels is
494 controlled by the Siah2 E3 ubiquitin ligase, thus regulation of Pard3a expression may be
495 due to a complex interplay between transcriptional and post-translation mechanisms. In
496 conclusion, further examination of Zeb1 function in neural progenitors and its relation to
497 other GZ exit pathways and the MET-like conceptual model may be useful not only in
498 understanding how normal GNPs transition to the CGN state, but also in understanding
499 the pathogenesis of pediatric cancers linked to defective GZ exit.

500

501

502 **Materials and Methods**

503 **Animals**

504 All mouse lines were maintained in standard conditions in accordance with guidelines
505 established and approved by Institutional Animal Care and Use Committee at St. Jude
506 Children's Research Hospital (protocol number = 483). B6N.129-*Ptch1*^{tm1Hahn}/J strain
507 mice were obtained from Jackson labs.

508 ***Plasmid vectors***

509 All cDNAs encoding protein of interest were commercially synthesized and subcloned
510 into pCIG2 by Genscript (Piscataway, NJ, USA). Expression plasmid for Pard3a,
511 Pard6a, Jam-C-Nectin3 and Fluorescent fusion proteins such as pCIG2 H2B-mCherry,
512 pCIG2 RFP-UTRCH, pCIG2 Centin2-Venus and pCIG2 JAM-C-pHluorin were
513 subcloned as previously described (75).

514 ***Preparation and nucleofection of CGNs***

515 CGNs were prepared as described(76). Briefly, cerebella were dissected from the
516 brains of P7 mice and pial layer removed; the tissue was treated with trypsin/DNase and
517 triturated into a single-cell suspension using fine-bore Pasteur pipettes. The suspension
518 was layered onto a discontinuous Percoll gradient and separated by centrifugation. The
519 small-cell fraction was then isolated. The resulting cultures routinely contain 95% CGNs
520 and 5% glia. For imaging experiments, expression vectors encoding fluorescently
521 labeled cytoskeletal proteins and pCIG2 expressing protein of interests were introduced
522 into granule neurons via Amaxa nucleofection, using the Amaxa mouse neuron
523 nucleofector kit per the manufacturer's instructions and program A030. The
524 concentration pCIG2 expression vectors used was determined such that increase in
525 protein expression was at least two fold. After cells recovered for 10 min from the
526 nucleofection, they were plated in either plated in 16 well slides for IHC or in movie
527 dishes (Mattek) coated with low concentrations of poly-L-ornithine to facilitate the
528 attachment of neurons to glial processes (according to methods established by (77)

529 ***Gene expression: RNA isolation, RT-PCR flow cytometry and Affymetrix arrays***

530 **RNA extraction and SYBR green real-time RT-PCR**

531 Total RNA for RT-PCR and microarray was isolated from either CGNs or whole
532 cerebellum at different developmental time points such as postnatal day such as p0, p4,
533 p7, p10, p15 by using the Ambion RNA Aqueous kit (Austin, TX). According to
534 manufacturer's instructions each sample was isolated in 40 μ l of elution buffer and
535 subjected to Dnase treatment (Ambion) to get rid of any genomic contamination.
536 Quantity and quality of the isolated RNA was checked using the Agilent 2100
537 Bioanalyzer with RNA 6000 Nano Chips (Agilent Technologies, Santa Clara, CA).
538 Primer sets for each gene were designed by using Primer Express Software (Applied
539 Biosystems, Foster City, CA) and synthesized (IDT, Coralville, IA). Sequences of the
540 primers are listed in See Table is Supplementary file 3A. Two-step real-time RT-PCR
541 was performed on the ABI PRISM 7900 Sequence Detection System by using random
542 hexamers and the TaqMan Reverse Transcription Reagents, and the SYBR Green PCR
543 Master Mix for the PCR step (Applied Biosystems) as described(78). Data were
544 normalized by the 18S ribosomal RNA expression levels in each sample.

545

546 **Fluorescence-activated cell sorting, Affymetrix Array and analysis**

547 To obtain a pure population of GNPs expressing the protein of interest, GNPs isolated
548 from cerebellum of postnatal day p7 mice were nucleofected with pCIG2 H2B-mCherry
549 (to label cells red [Control]) or mCherry with either Zeb1/Hes1, cultured for 24 hrs,
550 triturated into single cell suspension and labeled for DAPI. The viable mCherry positive

551 cells sorting was carried out in St. Jude shared resource flow cytometry facility at St.
552 Jude using BD Aria III SORP sorter. A bandpass 610/20 filter was used to detect
553 mCherry signals at an excitation of 561 nm laser. The cells were directly collected in
554 the lysis buffer and RNA was extracted as described in the previous section.

555 RNA for temporal developmental profiling was isolated directly after GNP isolation at
556 time point p0, p7 and p15 as well as FACS GNPs and further analyzed by the
557 microarray core facility at St Jude. RNA quality was determined by analysis on the
558 Agilent 2100 Bio-analyzer, and all samples had a RIN > 8. 100 ng of total RNA was
559 processed using the Affymetrix 3' IVT Express Kit. Biotin-labeled cRNAs were
560 hybridized to the Affymetrix GeneChip HT MG-430 PM array and washed, stained and
561 scanned on the GeneTitan system (Affymetrix). Data were summarized using Affymetrix
562 Expression Console software (v1.1) to apply the robust multi-array average (RMA)
563 algorithm (ArrayExpress accession number: E-MTAB-3557). The arrays are RMA-
564 normalized and batch corrected using R/ComBat. Unsupervised hierarchical clustering
565 analysis and principal component analysis was done using Spotfire and GeneMaths.
566 Differential expressed genes were analyzed using linear models algorithm (R/Limma).
567 Differentially expressed genes between Zeb1/Hes1-overexpression cells and GNPs at
568 different time point were selected using FDR corrected p-value (q value) of 0.05 and
569 fold change of 1.5 as the cutoff. GO analysis was done using DAVID Bioinformatics
570 Resource with the common up-regulated genes in Zeb1 and Hes1 over-expressed cells.

571 **RT² Profiler PCR arrays**

572 The Mouse EMT RT² Profiler PCR Array that profiles the expression of 84 key genes
573 was purchased from SABiosciences. Total RNA (1µg) isolated from the flow sorted GNP

574 isolated at p7 was used for screening by real-time PCR as per the manufacturer's
575 instructions. Target genes whose expression was differentially regulated (at least 2-fold
576 difference) by Zeb1 over expression were selected and are shown in tables in
577 Supplementary file 1A and B.

578 ***Chromatin immunoprecipitation: ChIP assay***

579 Chromatin immunoprecipitation (ChIP) was performed by using EZ ChIP reagents
580 (Millipore) in the presence of phosphatase and protease inhibitors according to the
581 manufacturer's instructions. Briefly, chromatin from CGNs ($\geq 1 \times 10^6$) was cross-linked
582 for 10 min at RT with 1% formaldehyde, sonically disrupted, diluted and precleared
583 before immunoprecipitation with either 5 µg of Zeb1 antibody or rabbit IgG as control at
584 4°C overnight. Protein G-agarose beads (60 µL/sample) were added and incubated for
585 a further 1 hour at 4°C. After washing with salt gradient stringent buffers, LiCl and TE
586 buffers, immunoprecipitated protein-DNA complexes were eluted in 200 µL of elution
587 buffer (50 mmol/L NaHCO₃, 1% SDS). Formaldehyde crosslinking was then reversed
588 by adding 8 µL of 5 mol/L NaCl and incubating at 65°C overnight. RNA and protein were
589 removed by sequential treatment with RNase for 30 min at 37°C and proteinase K at
590 45°C for 2 hours, respectively. Purified DNA fragments were then analysed with qRT-
591 PCR using specific primer for the promoter region see Table is Supplementary file 3B
592 and SYBR® Green PCR Master Mix (Applied Biosystems). The results were normalised
593 against the input control. Normalised data of three independent experiments were
594 averaged and are presented using fold change/enrichment of each promoter region
595 expressed as a ratio of PCR signal of samples to that of input. For example, fold

596 increase of promoter binding is defined as the ratio of Zeb1 binding DNA compared to
597 DNA precipitated with the IgG control antibody (set as a fixed value of 1.0).

598

599 ***ChIP-seq and bioinformatics analyses***

600 NS5 cells(79) were fixed sequentially with di(N-succimidyl) glutarate and 1%
601 formaldehyde in phosphate buffered saline (PBS) and then lysed, sonicated and
602 immunoprecipitated with anti-Zeb1 antibody (HPA027524, Sigma), as previously
603 described(80). DNA libraries were prepared from 10 ng of immunoprecipitated DNA
604 according to the standard Illumina ChIP-seq protocol and sequenced with Illumina
605 GAIx. Sequenced reads were processed after mapping with SAMTools for format
606 conversion and removal of PCR duplicates(81) and mapped to the mouse genome
607 (NCBI37/mm9) with Bowtie 0.12.7(82), resulting in 25 million uniquely mapped reads
608 (ArrayExpress accession number: E-MTAB-3560). Peak calling was performed with
609 MACS 1.4.1(83) (default parameters). Profiles of genomic regions were generated
610 using D-peaks source code(84). A *de novo* search for motifs enriched at peak summits
611 was done with Cisfinder(85) using default parameters and a background control set of
612 100 bp genomic regions located 3Kp upstream input regions. Calculation of P-values
613 for the association between binding events and deregulated genes was performed by
614 sampling the number of genes represented in the microarray 1000 times and assuming
615 a normal distribution. Annotation of binding events and association with genomic
616 features was performed with PeakAnalyzer(86) and the R/Bioconductor package
617 ChIPpeakanno(87).

618 **Cerebellar immunohistochemistry**

619 Postnatal brains collected at p7 and p15 were fixed by immersion in 4%
620 paraformaldehyde at 4°C for overnight followed by cryoprotection in PBS containing
621 30% sucrose. Histological sagittal sections were cut at 60 µm on a cryostat and pre-
622 blocked for 1 hr in PBS with 0.1% Triton X-100 and 10% normal donkey serum.
623 Sections were incubated overnight at 4°C with the primary antibodies followed by
624 appropriate Alexa labeled secondary antibody (Invitrogen) at 1:1000 for an hour before
625 mounting. Antigen retrieval was carried out for Meis1 staining.

626 **Immunocytochemistry of primary CGN cultures**

627 CGNs cultured *in vitro* for various times were washed with PBS, permeabilized with
628 Triton X-100 (0.1%) and blocked with normal donkey serum (10%). Primary and
629 secondary antibody staining was carried out in PBS plus 1% normal donkey serum. The
630 list of primary antibodies used in this study can be found in table in Supplementary file
631 3C. Alexa labeled secondary antibodies (Invitrogen) were used to detect primary
632 antibody stains. The slides were sealed with a coverslip using ProLong Gold mounting
633 media (Invitrogen).

634

635 ***Image and data analysis: neurite length measurement and differentiation assay***

636 CGN cultures were imaged with a Marianas Spinning Disk Confocal Microscope
637 (Intelligent Imaging Innovations) comprising a Zeiss Axio Observer microscope
638 equipped with 40×/1.0 NA (oil immersion) and 63×/1.4 NA (oil immersion)
639 PlanApochromat objectives. An Ultraview CSUX1 confocal head with 440 to 514 nm or

640 488/561/642 nm excitation filters and ImageEM-intensified CCD camera (Hamamatsu)
641 were used for high-resolution imaging.

642 Neurite length measurements were performed using the ruler function of SlideBook
643 software (Intelligent Imaging Innovations) by measuring the longest neurite from one
644 end to the longest neurite on the opposite end. At least three independent biological
645 replicates were done for each target gene. While measuring neurite length in the rescue
646 experiments, only CGNs that showed at least two fold increase in Zeb1 expression were
647 included for neurite measurement. Data was statistically analyzed using Microsoft Excel
648 and graphed using Kaleidagraph v4.03.

649

650 **Ki67 and p27 data analysis**

651 Result of Ki67 immunostaining is represented as percentage of positively stained ki67
652 nuclei (cut off 20-25 % staining intensity) among the total number of neurons present in
653 the image field. For Zeb1 overexpression and the epistasis studies only nuclei that
654 showed both Zeb1 expression and ki67 were counted as a positive over total number of
655 GNPs overexpressing Zeb1. Scoring involved counting at least 25 fields (X40 oil
656 objective) to a minimum of 150-200 neurons in each of three independent experiments

657

658 For assessment of differentiation p27 negative cells were counted and expressed as a
659 percentage of the total number of GNPs in the field. For analyzing p27 in the Zeb1
660 overexpression and epistasis experiments a scoring cut-off of 25% staining intensity for
661 p27 and concomitant expression for Zeb1 expression was considered and counted over
662 total number of Zeb1 overexpressing GNPs in the field.

663

664 ***Ex vivo cerebellar electroporation, organotypic slice culture and imaging***

665 P7 cerebella were dissected, soaked in endotoxin-free plasmid DNA suspended in
666 Hanks balanced salt solution (1-5 µg/µL of each DNA was generally used, pCIG2-
667 mCherryH2B was electroporated as a nuclear marker for migrating CGNs), transferred
668 to a CUY520-P5 platinum block petri dish electrode (Protech International) and
669 electroporated with a CUY21EDIT (Protech International) square wave electroporator
670 (80 V, 5 pulses, 50 ms pulse, 500 ms interval). Electroporated cerebella were
671 embedded in 4% low melting point agarose and 250 µm sagittal cerebellar slices were
672 prepared using a VT1200 Vibratome (Leica Microsystems). Slices were transferred to
673 Millicell tissue culture inserts (Millipore) and cultured in basal Eagle medium
674 supplemented with 2 mM L-glutamine, 0.5% glucose, 50 U/ml penicillin-streptomycin, 1x
675 B27 and 1x N2 supplements (Invitrogen) at the air-media interface for the times
676 indicated in the Figures. In experiments that assayed proliferation, 25 µM EdU was
677 added to culture medium and EdU incorporation was assayed by using the Click-iT
678 assay as per manufacturer instructions (Invitrogen).

679 Previous characterization of this method show that greater than 97% of cell manipulated
680 by this method are Pax6 positive CGNs in outer EGL(12). For analysis of fixed
681 specimens, slices were fixed 4% paraformaldehyde after 24 or 48 hrs of culture and
682 mounted on slides by using ProLong Gold (Invitrogen). Migration distance was
683 measured in fixed slices by measuring the distance between the cerebellar surface and
684 center of individual cell nuclei marked by mCherry-H2B. Central coordinates were
685 exported from SlideBook (Intelligent Imaging Innovations) into IGOR Pro (WaveMetrics

686 Inc.), where the distance of cells from the nearest cerebellar surface was measured and
687 logged. Statistical analysis used Microsoft Excel and was graphed by using
688 Kaleidagraph v4.03. For live-imaging analysis of the migration of H2B-mCherry labeled
689 CGNs, slice cultures were transferred at 28 hrs to the humidified chamber of the
690 spinning disk confocal microscope described above. Z-stacks (60-80 μ m width, ~20
691 sections per stack) were collected at multiple x, y stage positions every 15 min for 24-48
692 hrs.

693 **Tumor samples**

694 qRT-PCR analyses and IHC for Medulloblastoma studies were done on GNP-like tumor
695 cells purified from 6 different mouse tumors that developed around 20-35 week
696 in *Ptch1^{±/-}-Ink4c^{-/-}* mice and compared with GNPs were isolated from the cerebellum of
697 p7 mice.

698 **Western blotting**

699 P7 GNPs were cultured with or without SAG for 48 hrs, and thereafter processed to
700 obtain nuclear and cytoplasmic fractions using the Thermo NE-PER Nuclear and
701 Cytoplasmic Extraction Reagent. Nuclear lysates were denatured using LifeTech
702 NuPAGE sample reducing agent and LifeTech loading bufferheated to 75°C for 5
703 minutes. Samples were subjected to SDS-PAGE 4-12% Bis-Tris gel by LifeTech. The
704 proteins were then electroblotted on to polyvinylidene fluoride membranes using an iBlot
705 Gel Transfer Device (Invitrogen). Membrane was blocked for 1hr at RT with Odyssey
706 Blocking buffer diluted 1:2 and then incubated in rabbit anti Zeb1 (1:2000) (prestige)

707 antibody and anti-Fibrillarin-loading control (1:2000) overnight at 4°C. Odyssey
708 secondary antibodies (1:10000) was used for detecting proteins by using the Odyssey
709 Infrared Scanner.

710 **Statistical analysis**

711 All data were expressed as the mean ± SD or SE as appropriate. The Student's *t*-test
712 was used for comparing two groups, and the one-way analysis of variance and Holm-
713 Sidak posthoc test was used for multiple comparisons, with the level of statistical
714 significance set at p<0.01 unless otherwise specified. In migration rescue assays, if
715 rescuing conditions resulted in a χ^2 -test p-value > 0.8 when compared to controls, and t-
716 test p-value < 0.01 when compared to Zeb1 overexpression alone, then they were
717 considered a rescue.

718

719 **AUTHOR CONTRIBUTIONS**

720 SS carried out qRT-PCR, ChIP, expression arrays, *in vitro* analyses and the functional
721 screen. DH carried out *ex vivo* analyses and the functional screen. NT examined Zeb1
722 silencing phenotypes *ex vivo* and prepared all figures and statistical analyses. KK
723 carried out many proof of principle experiments in the initial phase of project
724 development. TO performed Ptch1 fl/fl experiments and developed the Zeb1 shmir. PR
725 carried out the NS5 ChIP-seq studies and developed the Zeb1 shRNA. AASFR carried
726 out bioinformatics comparison of NS5 and CGN expression data. GR analyzed Zeb1 in
727 human MB. MFR participated in conceptual study design, provided mouse MB
728 microarray data and coordinated mouse MB studies. DC designed and carried out NS5

729 ChIP-seq studies and designed bioinformatics comparison of NS5 and CGN expression
730 data. DJS conceived of the study, participated in its design and coordination and
731 performed all time-lapse studies. SS, DH, NT, TO, MR, DC, and DJS drafted or edited
732 the manuscript.

733

734 **ACKNOWLEDGEMENTS:** We thank Douglas Darling for sharing Zeb1 antibodies and
735 Chunxu Qu for analyzing Affymetrix Array data. Sharon Naron edited the manuscript.
736 The Solecki Laboratory is funded by the American Lebanese Syrian Associated
737 Charities (ALSAC), by grant #1-FY12-455 from the March of Dimes and by grant
738 1R01NS066936 from the National Institute Of Neurological Disorders (NINDS).

739 **Competing Interests**

740 None to declare for all authors.

741 **REFERENCES**

- 742 1. Shi SH, Jan LY, Jan YN. Hippocampal neuronal polarity specified by spatially localized
743 mPar3/mPar6 and PI 3-kinase activity. *Cell*. 2003 Jan 10;112(1):63-75. PubMed PMID:
744 12526794.
- 745 2. Solecki DJ, Model L, Gaetz J, Kapoor TM, Hatten ME. Par6alpha signaling controls
746 glial-guided neuronal migration. *Nat Neurosci*. 2004 Nov;7(11):1195-203. PubMed PMID:
747 15475953.
- 748 3. Kishi M, Pan YA, Crump JG, Sanes JR. Mammalian SAD kinases are required for
749 neuronal polarization. *Science (New York, N Y)*. 2005;307(5711):929-32. PubMed PMID:
750 Medline:15705853. English.
- 751 4. Cappello S, Attardo A, Wu X, Iwasato T, Itohara S, Wilsch-Brauninger M, et al. The
752 Rho-GTPase cdc42 regulates neural progenitor fate at the apical surface. *Nat Neurosci*. 2006
753 Sep;9(9):1099-107. PubMed PMID: 16892058.
- 754 5. Rasin MR, Gazula VR, Breunig JJ, Kwan KY, Johnson MB, Liu-Chen S, et al. Numb and
755 Numbl are required for maintenance of cadherin-based adhesion and polarity of neural
756 progenitors. *Nat Neurosci*. 2007 Jul;10(7):819-27. PubMed PMID: 17589506.
- 757 6. Shelly M, Cancedda L, Heilshorn S, Sumbre G, Poo MM. LKB1/STRAD promotes axon
758 initiation during neuronal polarization. *Cell*. 2007 May 4;129(3):565-77. PubMed PMID:
759 17482549.

- 760 7. Barnes AP, Lilley BN, Pan YA, Plummer LJ, Powell AW, Raines AN, et al. LKB1 and
761 SAD kinases define a pathway required for the polarization of cortical neurons. *Cell*. 2007 May
762 4;129(3):549-63. PubMed PMID: 17482548.
- 763 8. Bultje RS, Castaneda-Castellanos DR, Jan LY, Jan YN, Kriegstein AR, Shi SH.
764 Mammalian Par3 regulates progenitor cell asymmetric division via notch signaling in the
765 developing neocortex. *Neuron*. 2009 Jul 30;63(2):189-202. PubMed PMID: 19640478. Pubmed
766 Central PMCID: 2736606.
- 767 9. Hengst U, Deglincerti A, Kim HJ, Jeon NL, Jaffrey SR. Axonal elongation triggered by
768 stimulus-induced local translation of a polarity complex protein. *Nature cell biology*. 2009
769 Aug;11(8):1024-30. PubMed PMID: 19620967. Pubmed Central PMCID: 2724225.
- 770 10. Zhou P, Alfaro J, Chang EH, Zhao X, Porcionatto M, Segal RA. Numb links extracellular
771 cues to intracellular polarity machinery to promote chemotaxis. *Developmental cell*. 2011 May
772 17;20(5):610-22. PubMed PMID: 21571219. Pubmed Central PMCID: 3103748.
- 773 11. Chen S, Chen J, Shi H, Wei M, Castaneda-Castellanos DR, Bultje RS, et al. Regulation
774 of microtubule stability and organization by mammalian Par3 in specifying neuronal polarity.
775 *Developmental cell*. 2013 Jan 14;24(1):26-40. PubMed PMID: 23273878. Pubmed Central
776 PMCID: 3549028.
- 777 12. Famulski JK, Trivedi N, Howell D, Yang Y, Tong Y, Gilbertson R, et al. Siah regulation
778 of Pard3a controls neuronal cell adhesion during germinal zone exit. *Science*. 2010 Dec
779 24;330(6012):1834-8. PubMed PMID: 21109632. Pubmed Central PMCID: 3065828. Epub
780 2010/11/27. eng.
- 781 13. May-Simera H, Liu C. Neuronal Polarity and Neurological Disorders. *Journal of
782 Neurology and Translational Neuroscience*. 2013;2(1).
- 783 14. Barnes AP, Polleux F. Establishment of axon-dendrite polarity in developing neurons.
784 *Annu Rev Neurosci*. 2009;32:347-81. PubMed PMID: 19400726. Pubmed Central PMCID:
785 3170863.
- 786 15. Lewis TL, Jr., Courchet J, Polleux F. Cell biology in neuroscience: Cellular and
787 molecular mechanisms underlying axon formation, growth, and branching. *The Journal of cell
788 biology*. 2013;202(6):837-48. PubMed PMID: Medline:24043699. English.
- 789 16. Funahashi Y, Namba T, Nakamura S, Kaibuchi K. Neuronal polarization in vivo:
790 Growing in a complex environment. *Curr Opin Neurobiol*. 2014;27:215-23. PubMed PMID:
791 Medline:24800936. English.
- 792 17. de la Torre-Ubieta L, Bonni A. Transcriptional regulation of neuronal polarity and
793 morphogenesis in the mammalian brain. *Neuron*. 2011;72(1):22-40. PubMed PMID:
794 Medline:21982366. English.
- 795 18. Hirabayashi Y, Gotoh Y. Epigenetic control of neural precursor cell fate during
796 development. *Nature reviews Neuroscience*. 2010 Jun;11(6):377-88. PubMed PMID: 20485363.
- 797 19. Yamada T, Yang Y, Hemberg M, Yoshida T, Cho HY, Murphy JP, et al. Promoter
798 decommissioning by the NuRD chromatin remodeling complex triggers synaptic connectivity in
799 the mammalian brain. *Neuron*. 2014 Jul 2;83(1):122-34. PubMed PMID: 24991957. Pubmed
800 Central PMCID: 4266462.
- 801 20. Cooper JA. Molecules and mechanisms that regulate multipolar migration in the
802 intermediate zone. *Frontiers in cellular neuroscience*. 2014;8:386. PubMed PMID: 25452716.
803 Pubmed Central PMCID: 4231986.

- 804 21. Singh S, Solecki DJ. Polarity transitions during neurogenesis and germinal zone exit in
805 the developing central nervous system. *Frontiers in cellular neuroscience*. 2015;9:62. PubMed
806 PMID: 25852469. Pubmed Central PMCID: 4349153.
- 807 22. Vandewalle C, Van Roy F, Berx G. The role of the ZEB family of transcription factors in
808 development and disease. *Cellular and molecular life sciences : CMLS*. 2009 Mar;66(5):773-87.
809 PubMed PMID: 19011757.
- 810 23. Hatten ME, Roussel MF. Development and cancer of the cerebellum. *Trends Neurosci*.
811 2011 Mar;34(3):134-42. PubMed PMID: 21315459. Pubmed Central PMCID: 3051031.
- 812 24. Roussel MF, Hatten ME. Cerebellum development and medulloblastoma. *Current topics*
813 in developmental biology
- 814 2011;94:235-82. PubMed PMID: 21295689. Pubmed Central PMCID:
3213765.
- 815 25. Hatten ME. New directions in neuronal migration. *Science*. 2002 Sep 6;297(5587):1660-
816 3. PubMed PMID: 12215636.
- 817 26. Chedotal A. Should I stay or should I go? Becoming a granule cell. *Trends Neurosci*.
818 2010 Apr;33(4):163-72. PubMed PMID: 20138673.
- 819 27. Legue E, Riedel E, Joyner AL. Clonal analysis reveals granule cell behaviors and
820 compartmentalization that determine the folded morphology of the cerebellum. *Development*.
821 2015 May 1;142(9):1661-71. PubMed PMID: 25834018.
- 822 28. Goodrich LV, Milenkovic L, Higgins KM, Scott MP. Altered neural cell fates and
823 medulloblastoma in mouse patched mutants. *Science*. 1997 Aug 22;277(5329):1109-13. PubMed
824 PMID: 9262482.
- 825 29. Kim JY, Nelson AL, Algon SA, Graves O, Sturla LM, Goumnerova LC, et al.
826 Medulloblastoma tumorigenesis diverges from cerebellar granule cell differentiation in patched
827 heterozygous mice. *Dev Biol*. 2003 Nov 1;263(1):50-66. PubMed PMID: 14568546.
- 828 30. Yang ZJ, Ellis T, Markant SL, Read TA, Kessler JD, Bourboulas M, et al.
829 Medulloblastoma can be initiated by deletion of Patched in lineage-restricted progenitors or stem
830 cells. *Cancer cell*. 2008 Aug 12;14(2):135-45. PubMed PMID: 18691548. Pubmed Central
831 PMCID: 2538687.
- 832 31. Ayrault O, Zhao H, Zindy F, Qu C, Sherr CJ, Roussel MF. Atoh1 inhibits neuronal
833 differentiation and collaborates with Gli1 to generate medulloblastoma-initiating cells. *Cancer*
834 research. 2010 Jul 1;70(13):5618-27. PubMed PMID: 20516124. Pubmed Central PMCID:
835 2896438.
- 836 32. Takagi T, Moribe H, Kondoh H, Higashi Y. DeltaEF1, a zinc finger and homeodomain
837 transcription factor, is required for skeleton patterning in multiple lineages. *Development*
838 (Cambridge, England). 1998;125(1):21-31. PubMed PMID: Medline:9389660. English.
- 839 33. Liu Y, El-Naggar S, Darling DS, Higashi Y, Dean DC. Zeb1 links epithelial-
840 mesenchymal transition and cellular senescence. *Development*. 2008 Feb;135(3):579-88.
841 PubMed PMID: 18192284. Pubmed Central PMCID: 2507753.
- 842 34. Darling DS, Stearman RP, Qi Y, Qiu MS, Feller JP. Expression of Zfhep/deltaEF1
843 protein in palate, neural progenitors, and differentiated neurons. *Gene expression patterns : GEP*.
844 2003 Dec;3(6):709-17. PubMed PMID: 14643678. Pubmed Central PMCID: 3682426.
- 845 35. Spaderna S, Schmalhofer O, Wahlbuhl M, Dimmler A, Bauer K, Sultan A, et al. The
846 transcriptional repressor ZEB1 promotes metastasis and loss of cell polarity in cancer. *Cancer*
847 research. 2008 Jan 15;68(2):537-44. PubMed PMID: 18199550.
- 848 36. Aigner K, Dampier B, Descovich L, Mikula M, Sultan A, Schreiber M, et al. The
849 transcription factor ZEB1 (deltaEF1) promotes tumour cell dedifferentiation by repressing

- 850 master regulators of epithelial polarity. *Oncogene*. 2007 Oct 25;26(49):6979-88. PubMed PMID:
851 17486063. Pubmed Central PMCID: 2899859.
- 852 37. Roussel DL, Pearson CA, Gaber ZB, Miquelajauregui A, Li S, Portera-Cailliau C, et al.
853 Foxp-mediated suppression of N-cadherin regulates neuroepithelial character and progenitor
854 maintenance in the CNS. *Neuron*. 2012 Apr 26;74(2):314-30. PubMed PMID: 22542185.
855 Pubmed Central PMCID: 3444171.
- 856 38. Itoh Y, Moriyama Y, Hasegawa T, Endo TA, Toyoda T, Gotoh Y. Scratch regulates
857 neuronal migration onset via an epithelial-mesenchymal transition-like mechanism. *Nature
858 neuroscience*. 2013;16(4):416-25. PubMed PMID: Medline:23434913. English.
- 859 39. Barnes AP, Solecki D, Polleux F. New insights into the molecular mechanisms
860 specifying neuronal polarity in vivo. *Curr Opin Neurobiol*. 2008 Feb;18(1):44-52. PubMed
861 PMID: 18514505. Epub 2008/06/03. eng.
- 862 40. Maricich SM, Herrup K. Pax-2 expression defines a subset of GABAergic interneurons
863 and their precursors in the developing murine cerebellum. *J Neurobiol*. 1999 Nov 5;41(2):281-
864 94. PubMed PMID: 10512984.
- 865 41. Chung SH, Guo F, Jiang P, Pleasure DE, Deng W. Olig2/Plp-positive progenitor cells
866 give rise to Bergmann glia in the cerebellum. *Cell death & disease*. 2013;4:e546. PubMed PMID:
867 23492777. Pubmed Central PMCID: 3615735.
- 868 42. Flora A, Klisch TJ, Schuster G, Zoghbi HY. Deletion of Atoh1 disrupts Sonic Hedgehog
869 signaling in the developing cerebellum and prevents medulloblastoma. *Science*. 2009 Dec
870 4;326(5958):1424-7. PubMed PMID: 19965762. Pubmed Central PMCID: 3638077.
- 871 43. Solecki DJ, Liu XL, Tomoda T, Fang Y, Hatten ME. Activated Notch2 signaling inhibits
872 differentiation of cerebellar granule neuron precursors by maintaining proliferation. *Neuron*.
873 2001 Aug 30;31(4):557-68. PubMed PMID: 11545715.
- 874 44. Miyata T, Maeda T, Lee JE. NeuroD is required for differentiation of the granule cells in
875 the cerebellum and hippocampus. *Genes Dev*. 1999 Jul 1;13(13):1647-52. PubMed PMID:
876 10398678. Pubmed Central PMCID: 316850.
- 877 45. Iacopetti P, Michelini M, Stuckmann I, Obach B, Aaku-Saraste E, Huttner WB.
878 Expression of the antiproliferative gene TIS21 at the onset of neurogenesis identifies single
879 neuroepithelial cells that switch from proliferative to neuron-generating division. *Proc Natl Acad
880 Sci U S A*. 1999 Apr 13;96(8):4639-44. PubMed PMID: 10200315. Pubmed Central PMCID:
881 16385.
- 882 46. Xenaki D, Martin IB, Yoshida L, Ohyama K, Gennarini G, Grumet M, et al. F3/contactin
883 and TAG1 play antagonistic roles in the regulation of sonic hedgehog-induced cerebellar granule
884 neuron progenitor proliferation. *Development*. 2011 Feb;138(3):519-29. PubMed PMID:
885 21205796. Pubmed Central PMCID: 3014637.
- 886 47. Demyanenko GP, Schachner M, Anton E, Schmid R, Feng G, Sanes J, et al. Close
887 homolog of L1 modulates area-specific neuronal positioning and dendrite orientation in the
888 cerebral cortex. *Neuron*. 2004 Oct 28;44(3):423-37. PubMed PMID: 15504324.
- 889 48. Demyanenko GP, Halberstadt AI, Rao RS, Maness PF. CHL1 cooperates with PAK1-3 to
890 regulate morphological differentiation of embryonic cortical neurons. *Neuroscience*. 2010 Jan
891 13;165(1):107-15. PubMed PMID: 19819308. Pubmed Central PMCID: 2791357.
- 892 49. Bachmann A, Timmer M, Sierralta J, Pietrini G, Gundelfinger ED, Knust E, et al. Cell
893 type-specific recruitment of Drosophila Lin-7 to distinct MAGUK-based protein complexes
894 defines novel roles for Sdt and Dlg-S97. *J Cell Sci*. 2004 Apr 15;117(Pt 10):1899-909. PubMed
895 PMID: 15039455.

- 896 50. Wang W, Mullikin-Kilpatrick D, Crandall JE, Gronostajski RM, Litwack ED, Kilpatrick
897 DL. Nuclear factor I coordinates multiple phases of cerebellar granule cell development via
898 regulation of cell adhesion molecules. *J Neurosci*. 2007 Jun 6;27(23):6115-27. PubMed PMID:
899 17553984.
- 900 51. Gupta A, Sanada K, Miyamoto DT, Rovelstad S, Nadarajah B, Pearlman AL, et al.
901 Layering defect in p35 deficiency is linked to improper neuronal-glial interaction in radial
902 migration. *Nat Neurosci*. 2003 Dec;6(12):1284-91. PubMed PMID: 14608361.
- 903 52. Huard JM, Forster CC, Carter ML, Sicinski P, Ross ME. Cerebellar histogenesis is
904 disturbed in mice lacking cyclin D2. *Development*. 1999 May;126(9):1927-35. PubMed PMID:
905 10101126.
- 906 53. Wechsler-Reya RJ, Scott MP. Control of neuronal precursor proliferation in the
907 cerebellum by Sonic Hedgehog. *Neuron*. 1999 Jan;22(1):103-14. PubMed PMID: 10027293.
- 908 54. Pomeroy SL, Tamayo P, Gaasenbeek M, Sturla LM, Angelo M, McLaughlin ME, et al.
909 Prediction of central nervous system embryonal tumour outcome based on gene expression.
910 *Nature*. 2002 Jan 24;415(6870):436-42. PubMed PMID: 11807556.
- 911 55. Lee Y, Miller HL, Jensen P, Hernan R, Connelly M, Wetmore C, et al. A molecular
912 fingerprint for medulloblastoma. *Cancer research*. 2003 Sep 1;63(17):5428-37. PubMed PMID:
913 14500378.
- 914 56. Robinson G, Parker M, Kranenburg TA, Lu C, Chen X, Ding L, et al. Novel mutations
915 target distinct subgroups of medulloblastoma. *Nature*. 2012 Aug 2;488(7409):43-8. PubMed
916 PMID: 22722829. Pubmed Central PMCID: 3412905.
- 917 57. Northcott PA, Shih DJ, Peacock J, Garzia L, Morrissey AS, Zichner T, et al. Subgroup-
918 specific structural variation across 1,000 medulloblastoma genomes. *Nature*. 2012 Aug
919 2;488(7409):49-56. PubMed PMID: 22832581. Pubmed Central PMCID: 3683624.
- 920 58. Uziel T, Zindy F, Xie S, Lee Y, Forget A, Magdaleno S, et al. The tumor suppressors
921 Ink4c and p53 collaborate independently with Patched to suppress medulloblastoma formation.
922 *Genes Dev*. 2005 Nov 15;19(22):2656-67. PubMed PMID: 16260494.
- 923 59. Ellis T, Smyth I, Riley E, Graham S, Elliot K, Narang M, et al. Patched 1 conditional null
924 allele in mice. *Genesis*. 2003 Jul;36(3):158-61. PubMed PMID: 12872247.
- 925 60. Itoh Y, Tyssowski K, Gotoh Y. Transcriptional coupling of neuronal fate commitment
926 and the onset of migration. *Curr Opin Neurobiol*. 2013 Dec;23(6):957-64. PubMed PMID:
927 23973158.
- 928 61. Colman DR. Neuronal polarity and the epithelial metaphor. *Neuron*. 1999
929 Aug;23(4):649-51. PubMed PMID: 10482232.
- 930 62. Thier JP, Sleeman JP. Complex networks orchestrate epithelial-mesenchymal
931 transitions. *Nature reviews Molecular cell biology*. 2006;7(2):131-42.
- 932 63. Nelson WJ. Remodeling epithelial cell organization: transitions between front-rear and
933 apical-basal polarity. *Cold Spring Harbor perspectives in biology*. 2009 Jul;1(1):a000513.
934 PubMed PMID: 20066074. Pubmed Central PMCID: 2742086.
- 935 64. Hausmann B, Sievers J. Cerebellar external granule cells are attached to the basal lamina
936 from the onset of migration up to the end of their proliferative activity. *J Comp Neurol*. 1985
937 Nov 1;241(1):50-62. PubMed PMID: 4056112.
- 938 65. Rakic P. Neuron-glia relationship during granule cell migration in developing cerebellar
939 cortex. A Golgi and electronmicroscopic study in Macacus Rhesus. *J Comp Neurol*. 1971
940 Mar;141(3):283-312. PubMed PMID: 4101340.

- 941 66. Del Cerro MP, Snider RS. Studies on the developing cerebellum. II. The ultrastructure of
942 the external granular layer. *J Comp Neurol*. 1972 Feb;144(2):131-64. PubMed PMID: 5029131.
- 943 67. Uziel T, Karginov FV, Xie S, Parker JS, Wang YD, Gajjar A, et al. The miR-17~92
944 cluster collaborates with the Sonic Hedgehog pathway in medulloblastoma. *Proc Natl Acad Sci
U S A*. 2009 Feb 24;106(8):2812-7. PubMed PMID: 19196975. Pubmed Central PMCID:
946 2636735.
- 947 68. Heng JI, Nguyen L, Castro DS, Zimmer C, Wildner H, Armant O, et al. Neurogenin 2
948 controls cortical neuron migration through regulation of Rnd2. *Nature*. 2008 Sep
949 4;455(7209):114-8. PubMed PMID: 18690213.
- 950 69. Pacary E, Heng J, Azzarelli R, Riou P, Castro D, Lebel-Potter M, et al. Proneural
951 transcription factors regulate different steps of cortical neuron migration through Rnd-mediated
952 inhibition of RhoA signaling. *Neuron*. 2011 Mar 24;69(6):1069-84. PubMed PMID: 21435554.
953 Pubmed Central PMCID: 3383999.
- 954 70. Raffel C, Jenkins RB, Frederick L, Hebrink D, Alderete B, Fults DW, et al. Sporadic
955 medulloblastomas contain PTCH mutations. *Cancer research*. 1997 Mar 1;57(5):842-5. PubMed
956 PMID: 9041183.
- 957 71. Lam CW, Xie J, To KF, Ng HK, Lee KC, Yuen NW, et al. A frequent activated
958 smoothened mutation in sporadic basal cell carcinomas. *Oncogene*. 1999 Jan 21;18(3):833-6.
959 PubMed PMID: 9989836.
- 960 72. Taylor MD, Liu L, Raffel C, Hui CC, Mainprize TG, Zhang X, et al. Mutations in SUFU
961 predispose to medulloblastoma. *Nature genetics*. 2002 Jul;31(3):306-10. PubMed PMID:
962 12068298.
- 963 73. Hatten ME, Alder J, Zimmerman K, Heintz N. Genes involved in cerebellar cell
964 specification and differentiation. *Curr Opin Neurobiol*. 1997 Feb;7(1):40-7. PubMed PMID:
965 9039803.
- 966 74. Choi Y, Borghesani PR, Chan JA, Segal RA. Migration from a mitogenic niche promotes
967 cell-cycle exit. *J Neurosci*. 2005 Nov 9;25(45):10437-45. PubMed PMID: 16280582.
- 968 75. Solecki DJ, Trivedi N, Govek EE, Kerekes RA, Gleason SS, Hatten ME. Myosin II
969 motors and F-actin dynamics drive the coordinated movement of the centrosome and soma
970 during CNS glial-guided neuronal migration. *Neuron*. 2009 Jul 16;63(1):63-80. PubMed PMID:
971 19607793. Pubmed Central PMCID: 2737100.
- 972 76. Hatten ME. Neuronal regulation of astroglial morphology and proliferation in vitro. *J
973 Cell Biol*. 1985 Feb;100(2):384-96. PubMed PMID: 3881455.
- 974 77. Edmondson JC, Hatten ME. Glial-guided granule neuron migration in vitro: a high-
975 resolution time-lapse video microscopic study. *J Neurosci*. 1987 Jun;7(6):1928-34. PubMed
976 PMID: 3598656.
- 977 78. Singh S, Vinson C, Gurley CM, Nolen GT, Beggs ML, Nagarajan R, et al. Impaired Wnt
978 signaling in embryonal rhabdomyosarcoma cells from p53/c-fos double mutant mice. *The
979 American journal of pathology*. 2010 Oct;177(4):2055-66. PubMed PMID: 20829439. Pubmed
980 Central PMCID: 2947299.
- 981 79. Pollard SM, Conti L, Sun Y, Goffredo D, Smith A. Adherent neural stem (NS) cells from
982 fetal and adult forebrain. *Cerebral cortex*. 2006 Jul;16 Suppl 1:i112-20. PubMed PMID:
983 16766697.
- 984 80. Castro DS, Martynoga B, Parras C, Ramesh V, Pacary E, Johnston C, et al. A novel
985 function of the proneural factor Ascl1 in progenitor proliferation identified by genome-wide

- 986 characterization of its targets. *Genes Dev.* 2011 May 1;25(9):930-45. PubMed PMID: 21536733.
987 Pubmed Central PMCID: 3084027.
- 988 81. Li H, Handsaker B, Wysoker A, Fennell T, Ruan J, Homer N, et al. The Sequence
989 Alignment/Map format and SAMtools. *Bioinformatics*. 2009 Aug 15;25(16):2078-9. PubMed
990 PMID: 19505943. Pubmed Central PMCID: 2723002.
- 991 82. Langmead B, Trapnell C, Pop M, Salzberg SL. Ultrafast and memory-efficient alignment
992 of short DNA sequences to the human genome. *Genome biology*. 2009;10(3):R25. PubMed
993 PMID: 19261174. Pubmed Central PMCID: 2690996.
- 994 83. Zhang Y, Liu T, Meyer CA, Eeckhoute J, Johnson DS, Bernstein BE, et al. Model-based
995 analysis of ChIP-Seq (MACS). *Genome biology*. 2008;9(9):R137. PubMed PMID: 18798982.
996 Pubmed Central PMCID: 2592715.
- 997 84. Brohee S, Bontempi G. D-peaks: a visual tool to display ChIP-seq peaks along the
998 genome. *Transcription*. 2012 Sep-Oct;3(5):255-9. PubMed PMID: 23132505. Pubmed Central
999 PMCID: 3632623.
- 1000 85. Sharov AA, Ko MS. Exhaustive search for over-represented DNA sequence motifs with
1001 CisFinder. *DNA research : an international journal for rapid publication of reports on genes and*
1002 *genomes*. 2009 Oct;16(5):261-73. PubMed PMID: 19740934. Pubmed Central PMCID:
1003 2762409.
- 1004 86. Salmon-Divon M, Dvinge H, Tammoja K, Bertone P. PeakAnalyzer: genome-wide
1005 annotation of chromatin binding and modification loci. *BMC bioinformatics*. 2010;11:415.
1006 PubMed PMID: 20691053. Pubmed Central PMCID: 2923140.
- 1007 87. Zhu LJ, Gazin C, Lawson ND, Pages H, Lin SM, Lapointe DS, et al. ChIPpeakAnno: a
1008 Bioconductor package to annotate ChIP-seq and ChIP-chip data. *BMC bioinformatics*.
1009 2010;11:237. PubMed PMID: 20459804. Pubmed Central PMCID: 3098059.
- 1010
- 1011
- 1012

1013 **FIGURE LEGENDS**

1014 **Figure 1. Zeb1 Is the Primary EMT Regulator Expressed in the Developing**
1015 **Cerebellum.**

1016 a. qRT-PCR shows that Zeb1 mRNA is more abundant than other EMT factors (Twist,
1017 Snail1, Snail2) in GNPs. Zeb1 mRNA diminishes in GNPs at P10 and P15 (Zeb mRNA
1018 was significantly different at all times, t-test p<0.01).

1019 b. Immunohistochemistry in P7 and P15 cerebellum shows Zeb1 (red) GNP expression
1020 at P7 coincident with that of Ki67, Meis1/2 and Siah2 (green) but complementary to the
1021 p27Kip marker (green). Zeb1 protein diminishes at P15.

1022 c. qRT-PCR shows increasing *Pard6a* and *Prkcz* mRNA as GNPs at P10 and P15.

1023 d. Immunohistochemistry in the P7 cerebellum of *Pard6a*-EGFP BAC transgenic mice
1024 shows little *Pard6a* promoter activity (green) in the outer EGL but elevated activity in the
1025 inner EGL with TAG1-positive CGNs (red).

1026 **Figure 2. Zeb1 Gain- or Loss-of-Function Determines GNP Differentiation.**

1027 a. Micrographs of purified CGNs nucleofected with Centrin2-Venus alone (green) or
1028 Myc-Zeb1 (magenta). After 24h in culture, control cells extend long neurites ($\bar{x} = 139.8 \pm$
1029 $13.3 \mu\text{m}$. n= 1045 cells), while Zeb1-expressing cells have short neurites ($\bar{x}= 59.6 \pm 3.0$
1030 μm , n= 1164 cells, χ^2 test, p<0.01).

1031 b. Micrographs of purified CGNs nucleofected with Centrin2-Venus (green) cytoplasmic
1032 marker and Myc-Zeb1. After 24h, levels of p27 labeling decreased, while that of Ki67
1033 and Atoh1 increased (t-test all conditions p<0.05). C,D. P7 EGL was co-electroporated
1034 with indicated vector and H2B-mCherry. After 24 (C) or 48 (D) h of ex vivo culture, the

1035 migration distance of labeled CGN from the pial layer (dashed line) was analyzed in 3
1036 experiments. Histograms show migration distributions. Zeb1-silenced cells incorporated
1037 EdU at lower rates than control cells.

1038 c. Most control shRNA-expressing cells (black) remain within the EGL (dashed lines, $\bar{x}=$
1039 $34.2 \pm 10.5 \mu\text{m}$) at 24h, while Zeb1-silenced cells pre-maturely enter the ML and IGL
1040 ($\bar{x}=67.5 \pm 18.1 \mu\text{m}$).

1041 d. Control cells (black) entered the ML and IGL by 48h ($\bar{x}=75.2 \pm 3.5 \mu\text{m}$), while Zeb1-
1042 expressing cells remain within the EGL ($\bar{x}=40.2 \pm 6.0 \mu\text{m}$). T-tests and χ^2 test showed
1043 significant differences in both conditions ($p<0.01$, $n= 4500$ to 9700 cells).

1044 e. Immunohistochemistry in E17.5 cerebellum of wild type and Zeb1 mutant embryos
1045 shows the expected absence of Zeb1 expression in mutant embryos. Moreover,
1046 increased expression of Tag1 and NeuN differentiation markers is observed in the
1047 absence of Zeb1.

1048 **Figure 3. Zeb1 Transcriptionally Represses Neuronal Differentiation, Cell Polarity,
1049 and Cell Adhesion Genes.**

1050 a. Schematic of procedure used to produce pure populations of CGNs for array studies.
1051 b. Heat map of the transcriptomes of GNPs and CGNs purified from P0, P7, and P15
1052 compared to pure populations of control (e.g. H2B-mCherry vector alone), Zeb1-
1053 expressing (e.g. H2B-mCherry and Zeb1 vector) and HES1-expressing (e.g. H2B-
1054 mCherry and HES1 vector) GNPs cultured for 24h *in vitro*. Yellow rectangle highlights
1055 genes whose expression increases with development and are repressed by Zeb1.

1056 c. qRT-PCR shows that ectopic Zeb1 expression inhibits transcription of most of the
1057 panel of CGN differentiation markers examined.

1058 d. Immunohistochemistry in P7 cerebellum shows Zeb1 (red) and Ki67 (green)
1059 expression complementary with expression of the Lin7a, Sorl1, Cdk5r1, Chl1, Dlg2 and
1060 Pard6a (red) CGN markers.

1061 **Figure 4. Zeb1 Binds to the Genomic Loci of Target Genes Identified in the**
1062 **Expression Screen.**

1063 a. Zeb1 binding events are significantly associated with down-regulated genes (right)
1064 but not with up-regulated genes (left) between the NS5 CHIP-Seq and CGN expression
1065 array data. Red bars: total number of binding events associated with each group of
1066 genes; boxplots: distribution of binding events associations with 1000 random sets of
1067 genes. Test data are represented as a boxplot showing the test median and 1st and 3rd
1068 quartiles; whiskers are ± 1.5 the interquartile range.

1069 b. Biological processes representing clusters of gene ontology terms enriched among
1070 genes directly targeted by Zeb1. Parentheses show number of genes associated with
1071 each term.

1072 c. Heat-map displaying the cumulative fraction of deregulated genes that are directly
1073 regulated by Zeb1 (up-top left panel; down-bottom left panel). Transcripts are divided in
1074 equal bins of decreasing expression fold change and plotted against Zeb1 binding
1075 events with increasing p-value. Control: 100 sets of random binding events (right
1076 panels, the mean value shown).

1077 d. CHIP PCR Validation of Zeb1 binding in P7 GNPs. The schematic on the left displays
1078 gene structure. Exons are pink rectangles, Zeb1 binding unoccupied motifs are colored
1079 light green and validated Zeb1 binding sites are colored dark green. The graph on the
1080 right shows fold enrichment at the listed genes.

1081 **Figure 5. Restored Expression of Zeb1-Target Genes Rescues Neurite Extension**
1082 **and CGN Differentiation Status *in Vitro*.** The rectangular images show representative
1083 morphological information and myc-Zeb1 expression; box plot below each quantifies
1084 neurite lengths in each experimental condition. On average control cells extended
1085 neurites $115.4 \pm 17.7 \mu\text{m}$ [$\bar{x} \pm \text{sd}$] compared to $55.2 \pm 2.6 \mu\text{m}$. Asterisks indicate
1086 conditions significantly different to the Zeb1 data as determined by t-test ($p < 0.01$).
1087 Images on right show representative Ki67 or p27 labeling, quantified below. Asterisks
1088 indicate statistically significant rescue of the Zeb1 phenotype by target expression
1089 determined by t-test ($p < 0.01$).

1090 **Figure 6. Restored Expression of Zeb1 Target Genes Rescues GNP Proliferation,**
1091 **GZ Exit and IGL-Directed Migration in *ex Vivo* Cerebellar Slices.** a Rectangles show
1092 representative P7 EGL slice images assessing GZ exit and IGL-directed migration.
1093 Labeled cell (black) migrate from the lateral surface (dashed line) to the IGL (to the
1094 right). Below each image is a cumulative distribution plot of all cells relative to a $450 \mu\text{m}$
1095 scale. Arrowhead indicates the 99th percentile of the total population. Control cells
1096 migrated $74.0 \pm 8.3 \mu\text{m}$ ($\bar{x} \pm \text{sd}$) while Zeb1 migrated $42.4 \pm 7.6 \mu\text{m}$. Images at right
1097 show representative EdU labeling with % labeling index. A statistically significant rescue
1098 of a Zeb1 phenotype in the slice migration assay is indicated by the presence of $p > 0.01$
1099 (t-test mean migration distance vs. control). Zeb1 and additional target expression

1100 conditions had a p-value < 0.01 vs. control indicating GZ was not rescued. Asterix
1101 indicates a statistical difference of EdU incorporation between Zeb1 and target
1102 expression condition by t-test [both p<0.01]). Reduced EdU labeling indicates a rescue
1103 of elevated proliferation in the Zeb1 gain of function condition. b Average migration
1104 distance shown in accompanying graph, a Student's t-test shows rescue conditions
1105 (Pard6a, Pard3a, Chl1, Jam/Nec, and Lin7a) with a p value>0.01 indicating no statistical
1106 difference from the control. Zeb1 alone and Zeb1 plus Dlg2, Sorl1, Blhle40, Cdh1,
1107 Nfib, Flt1 or Cdk5r1 migration differences were statistically lower than the control (t-test
1108 p<0.01), indicating GZ was not rescued with these targets.

1109 **Figure 7. Pard6a and Chl1 rescue neuronal differentiation in the Zeb1 gain-of-**
1110 **function context.** Cultured CGNs were nucleofected with a marker plasmid encoding
1111 H2B mCherry (or Centrin2-Venus in Panel c) alone or in combination with plasmids
1112 encoding Myc-Zeb1 plus single plasmids encoding *Pard6a* or *Chl1* in our array
1113 expression screen. After 24 h in culture, nucleofected cells were FACS sorted to isolate
1114 mRNA (a, b, c) or stained with antibodies to highlight morphology/Atoh1 expression (c).
1115 a. qRT-PCR analyses shows that: 1) Pard6a and *Pard3a* expression continues to be
1116 suppressed in Chl1 rescued GNPs and 2) Pard3 and Chl1 expression continues to be
1117 suppressed by Zeb1 Pard6a rescued GNPs. NS=not shown. b. qRT-PCR analyses
1118 shows that Zeb1 gain-of-function induced CyclinD1 and CyclinD2 mRNA expression
1119 and that both restored expression of Chl1 and Pard6a reduces D-type cyclin
1120 expression. c. qRT-PCR analyses shows that Zeb1 gain-of-function mildly induced
1121 Atoh1 mRNA expression. While Chl1 and Pard6a rescue have little affect on Atoh1

1122 mRNA expression, restored expression of both these genes strongly reduce Atoh1
1123 protein expression detected by immunocytochemistry.

1124 **Figure 8. Zeb1 Expression Is Linked to SHH Signaling, and Restoring Polarity of**
1125 **Ptch1-Deficient GNPs Rescues GZ Exit.**

1126 a. GNPs were cultured in the presence or absence of SAG, a small-molecule agonist of
1127 SHH, fixed and stained for DAPI (blue), Zeb1 (red) or the Zeb1 targets Pard6a, Chl1
1128 and Dlg2. Zeb1 expression was maintained, but Zeb1 target expression diminished.

1129 b. Western blotting with anti-Zeb1 confirmed that Zeb1 expression was maintained in
1130 the presence of SAG. Fibrillarin was loading control (t-test, p<0.01).

1131 c. Immunohistochemistry shows maintained expression of Zeb1 (red) in a Ptch1+/-,
1132 Cdkn2c-/- SHH-type mouse MB; Zeb1 expression is complementary to Tuji1 staining
1133 (green).

1134 d. qRT-PCR of mRNA from Ptch1+/-, Cdkn2c-/- mouse MBs shows much higher Zeb1
1135 mRNA expression in MB cells than in P7 GNPs. Most of the targets in our screen are
1136 expressed at a lower level in SHH MB than in P7 GNPs.

1137 e. *Zeb1* mRNA expression in 4 MB subgroups. Data set includes 74 MBs (WNT n=8;
1138 SHH n=11; G3 n=17; G4 n=38) profiled on the Affymetrix U133plus2 array.

1139 f. The migration distance of CGNs (black dots) from the pial layer (dashed line) was
1140 analyzed(n = 8,800 to 11,300 cells). Control cells expressing catalytically inactive Cre
1141 enter the ML and IGL ($71.2 \pm 7.8 \mu\text{m}$ [$\bar{x} \pm \text{sd}$]), while Ptch1-deficient GNPs expressing
1142 wild-type Cre remain within the EGL ($41.4 \pm 5.8 \mu\text{m}$). Zeb1 silencing and restored
1143 expression of Pard6a, Chl1 and Lin7a rescued the defective GZ exit (Asterisks indicate

1144 conditions where rescue observed (χ^2 test vs Cre mutant, $p>0.8$; t-test vs Cre WT,
1145 $p<0.01$). Below each image is a cumulative distribution plot showing the area relative to
1146 a 450 μm scale. Arrowhead indicates 99th population percentile.
1147 g. Average migration distance shown in accompanying graph, a Student's t-test shows
1148 rescue conditions with a p value <0.01 vs Cre wild type.

1149 **Figure 9. Model Comparing MET to GNP Differentiation.** **a** Mesenchymal-epithelial
1150 transition. Left: Mesenchymal cells are nonpolar, highly motile, with prominent cell-
1151 matrix contacts. Right: epithelial cells possess apical-basal polarity. Apical membrane
1152 (pink) is separated from basolateral and basal membranes by tight junctions (parallel
1153 blue rectangles) and adherens (blue springs) junctions. MET-EMT balance is controlled
1154 by antagonism between transcriptional regulators and polarity genes (center panel). **b**
1155 Left: GNP. As in MET, GNPs lose Zeb1 expression as they differentiate, relieving
1156 polarity gene repression. Center panel: Change in gene expression with GNP
1157 differentiation to CGNs. Right: CGNs morphologically mature, exit their GZ and make
1158 contacts with other CGNs or glia (blue springs depict adhesion to grey glial fiber). **c**
1159 Transition from tangential migration within the EGL by GNPs and nascent CGNs to
1160 radial migration (red arrows) by polarized T-shaped CGNs is MET-like, given falling
1161 Zeb1 expression (red to grey nuclei). Blue springs depict neuron-glial adhesions.
1162 Elevated SHH signaling drives Zeb1 expression to delay GZ exit at early stage of MB
1163 tumorigenesis.

1164 **Figure Supplement Legends**

1165 **Figure 1-figure supplement 1. Zeb1 is expressed in Pax2 and Olig2 positive**
1166 **progenitors in the developing cerebellar white matter.** Immunohistochemistry in P7

1167 cerebellum shows Zeb1 (green) expression at P7 partially overlaps with (a) Pax2 and
1168 (b) Olig2 in cerebellar white matter. This indicates that Zeb1 positive cells located in
1169 deeper cerebellar layers are interneuronal- or oligodendrocyte/glial-progenitors, not IGL
1170 resident CGNs.

1171

1172 **Figure 2-figure supplement 1. In depth quantitation of slice migration assays from**
1173 **Figure 2.** P7 EGL was co-electroporated with the indicated expression constructs and
1174 H2B-mCherry. After 24 (**a-d**) or 48 (**e-f**) hours of *ex vivo* culture, CGN migration
1175 distance was analyzed in 3 imaging experiments. Red overlay indicates the average
1176 migration distribution of control cells (error bar, SD). (**a, b**) Most control (n = 7,358 cells)
1177 migrated $34.2 \pm 10.1 \mu\text{m}$ [$\bar{x} \pm \text{sd}$] at 24 h, while Zeb1-silenced (n = 4,693 cells) migrated
1178 an Av. distance of $67.5 \pm 18.1 \mu\text{m}$. χ^2 analysis showed distribution of data to be
1179 significantly different ($p < 0.01$). (**c**) Binning distribution of the second mir30 based
1180 shRNA 846 used to confirm the precocious migration associated with Zeb1 silencing
1181 displayed in Figure 2C (n = 4879 cells). (**d**) Representative image of the mir30 based
1182 shRNA 846 illustrating Zeb1 silencing with a miRNA based shRNA also spurs GZ exit.
1183 (**e,f**) While control (n = 9,744 cells) cells entered the ML and IGL after 48 h (av distance
1184 = $75.2 \pm 3.5 \mu\text{m}$), However, Zeb1 (n = 5,359 cells) over-expressing cells remained in the
1185 EGL (Av. distance migrated = $40.2 \pm 6.0 \mu\text{m}$), which was shown to be significantly
1186 different by both χ^2 analysis and t-test ($p < 0.03$). (**g**) Summary of average distance
1187 migrated for the Zeb1-silencing and over-expression.

1188

1189 **Figure 2-figure supplement 2. shRNA knockdown of Zeb1.** **a** Immunoblots of lysates
1190 of NS5 cells transduced with shLuc or shZeb1. Zeb1 levels are lower than control NS5
1191 cell or cells expression a luciferase control shRNA. shZeb1 was used in Figure 2. **b**
1192 Immunoblots of lysates of HEK293 cells expressing Myc-Zeb1 with or without the
1193 corresponding shmiRNA constructs. After 48 h Myc-Zeb1 protein levels are substantially
1194 less than those in controls, actin was loading control. The Zeb1 shmiRNA was used in
1195 Figure 7.

1196

1197 **Figure 3-figure supplement 1. PCA analysis of array experiments shown in Figure**
1198 **3.** Principal component analysis (PCA) of Zeb1, Hes1-overexpression GNPs, controls and
1199 cerebellum granule neuron (CGN) cells purified at P0, P7 and P15. Total of 40.9% of variation
1200 among these samples can be explained by the first three component (PCA1 = 20.2%, PCA2 =
1201 10.6%, PCA3 = 10.1%). Hes1 samples are well separated from the rest along the first component
1202 and Zeb1 are separated from the controls along PCA3. Comparing with the Hes/Zeb controls, if
1203 the distance between the centroids of P7 CGNs and the control samples is 1, the distance for P0
1204 CGNs, P15 CGNs, Zeb1 samples and Hes1 samples are 1.3, 1.2, 1.2 and 2.4 indicating that the P7
1205 CGNs are most similar to the control samples.

1206

1207 **Figure 3-figure supplement 2. PCA demonstrating purity of GNPs/CGNs prepared**
1208 **at different developmental stages from Figure 3.** Principal component analysis (PCA) of
1209 GNP/CGN cells purified at P0, P7 and P15, compared to purified cerebellar glial cells. Variation
1210 among these samples can be explained by the first three components (PCA1 = 35.3%, PCA2 =
1211 15.4%, PCA3 = 9.84%). The purified glial cells are well separated indicating low levels of this

1212 most common contaminating cell population. The purified cells from each developmental stage
1213 are well clustered statically verifying the consistency of the purification procedure at the level of
1214 the whole transcriptome. P0 and P7 are most similar. The separation of P15 cells from the
1215 earlier developmental stages is on a principle component axis that unique from the purified glial
1216 cell population, indicating the differences are related to developmental changes in the cell
1217 population than contamination with a non-GNP/CGN cell population.

1218

1219

1220 **Figure 3-figure supplement 3. qRT-PCR analysis of Zeb1 target mRNA expression**
1221 **in GNP s or whole cerebellum.** RNA from purified GNP s (blue bars) or whole
1222 cerebellum (red bars) was extracted at p0, p7, and p15. qRT-PCR shows validate Zeb1
1223 target mRNA expression increases as GNP s mature. Cdk5r1 expression declines as
1224 GNP s mature.

1225

1226

1227

1228 **Figure 4-figure supplement 1. Overview of Zeb1 ChIP-Seq dataset in NS5 neural**
1229 **stem cells.**

1230 a. Location of Zeb1 binding events respective to the closest annotated TSS. b.
1231 Locations of Zeb1 binding events respective to various genomic features. c. Density plot
1232 of Zeb1 ChIP-seq reads mapping to the 4 Kb genomic regions surrounding peak
1233 summits. Signal intensity represents the ChIP-seq normalized tag count (left). Total
1234 bound sites were divided in 10 bins and the top motif found enriched at vicinity of

1235 summits is shown for each bin, with respective fold enrichment over genomic
1236 background (middle). The frequency of E-box motif is shown, centered on peak summits
1237 (right).

1238

1239 **Figure 4-figure supplement 2. Annotated ChIP peaks in polarity genes and**
1240 **putative Zeb1 targets identified in NS5 data set.** Visual representation of Zeb1 ChIP-
1241 seq enrichment in the vicinity of various putative Zeb1 targets. UTRs are represented as
1242 red rectangles, translated exons as black rectangles and the direction of transcription of
1243 a locus is represented by an arrow. The graph below each gene indicate the relative
1244 Zeb1 ChIP-Seq reads per million at each genomic position near the displayed genes. a.
1245 Shows Zeb1 binding enrichment at core PAR complex genes. Each core member of the
1246 PAR complex contains a region of enriched Zeb1 binding near Exon 1. b. Shows Zeb1,
1247 Chl1 and Limk2 genes. A scale bar indicates that size of each locus.

1248

1249 **Figure 6-figure supplement 1. In depth quantitation of slice migration assays from**
1250 **Figure 6.** P7 EGL was co-electroporated with the indicated expression constructs and
1251 H2B-mCherry. After 48 hours of *ex vivo* culture, CGN migration distance was analyzed
1252 in 3 imaging experiments. Red overlay indicates the average migration distribution of
1253 control cells (error bar, SD). While control (13,064 cells, $74.0 \pm 8.3 \mu\text{m}$ [$n, \bar{x} \pm \text{sd}$]) cells
1254 entered the ML and IGL after 48 h and Zeb1 over-expressing cells (13,424 cells, $42.4 \pm$
1255 $7.6 \mu\text{m}$) remained in the EGL, Addition of Pard6a (3,886 cells, $79.8 \pm 5.2 \mu\text{m}$), Pard3a
1256 (8,622 cells, $73.9 \pm 4.5 \mu\text{m}$), Jam/Nectin (11,333 cells, $71.7 \pm 5.5 \mu\text{m}$), Chl1 (3,006
1257 calls, $79.4 \pm 6.9 \mu\text{m}$) to Zeb1-expressing CGNs restored migration, suggesting that the

1258 Zeb1 migration phenotype are dependent on key polarity or cell adhesion molecule
1259 repression. Note: the criteria for rescue was set if the condition resulted in cell
1260 distribution that was 80% similar to the Control distribution (χ^2 -test $p>0.8$) and the
1261 average migration distance was less than 3% similar than the Zeb1 condition. Control
1262 vs Zeb1, [χ^2 test] $p(\chi^2) = 1.9 \times 10^{-7}$, [t-test] $p(t) = 6.44 \times 10^{-5}$. Control vs Pard6a $p(\chi^2) =$
1263 0.96, $p(t) = 3.68 \times 10^{-6}$. Control vs Pard3a $p(\chi^2) = 0.99$, $p(t) = 5.67 \times 10^{-5}$. Control vs
1264 Jam/Nec $p(\chi^2) = 0.98$, $p(t) = 3.67 \times 10^{-4}$. Control vs Chl1 $p(\chi^2) = 0.98$, $p(t) = 3.68 \times 10^{-6}$.
1265 Control vs Lin7a $p(\chi^2) = 0.84$, $p(t) = 0.02$. Control vs Dlg1 $p(\chi^2) = 0.25$, $p(t) = 0.06$.
1266 Control vs Sorl1 $p(\chi^2) = 0.04$, $p(t) = 0.01$. Control vs Blhle40 $p(\chi^2) = 0.13$, $p(t) = 0.06$.
1267 Control vs Cdh1 $p(\chi^2) = 5.57 \times 10^{-13}$, $p(t) = 0.44$. Control vs Flt1 $p(\chi^2) = 1.70 \times 10^{-4}$, $p(t)$
1268 = 0.27. Control vs Cdk5r1 $p(\chi^2) = 0.31$, $p(t) = 0.01$.

1269

1270 **Figure 6-figure supplement 2. Longer term ex vivo epistasis analysis.** P7 EGL was
1271 co-electroporated with the indicated expression constructs and H2B-mCherry. After 72
1272 hours of ex vivo culture, CGN migration distance was analyzed for a minimum of 4000
1273 nucleofected cells in each experimental condition. Red overlay indicates the average
1274 migration distribution of control cells (error bar, SD). While control cells entered the ML
1275 and IGL after 72 h, Zeb1 over-expressing cells remained in the EGL even with longer-
1276 term incubation. *Blhle40* expression, but not *Cdh1*, *Cdk5r1* and *Sorl1*, significantly
1277 restores IGL-directed migration of the context of Zeb1 gain-of-function (determined by
1278 Student t-test).

1279

1280 **Figure 7-figure supplement 1. Immunocytochemical analysis of Chl1 expression**
1281 **in Control, Zeb1-expressing or Pard6a and Pard3 rescued CGNs.** Dissociated
1282 CGNs were prepared and nucleofected with the indicated expression constructs. 18
1283 hours post-nucleofection, cultures were fixed and stained with antibodies recognizing
1284 EGFP and Chl1. Control neurons express robust levels of Chl1 protein in their somas
1285 and proximal leading process. In contrast, Zeb1 expressing as well as Pard6a or Pard3
1286 rescued cells expressed lower amounts of Chl1 immunoreactivity.

1287

1288 **Figure 8-figure supplement 1. In depth quantitation of slice migration assays from**
1289 **Figure 8.** P7 EGL of Ptch1 flox/flox animals was co-electroporated with the indicated
1290 expression constructs and H2B-mCherry. After 48 hours of *ex vivo* culture, CGN
1291 migration distance was analyzed in 3 imaging experiments. Red overlay indicates the
1292 average migration distribution of control cells (error bar, SD). While Cre Mutant (n =
1293 9,471 cells) cells entered the ML and IGL after 48 hrs and Cre wild type (n = 9,872)
1294 over-expressing cells remained in the EGL, Zeb1 silencing (n = 11,383) or addition of
1295 Pard6a (n = 8,839), Lin7a (n = 10,543), or Chl1 (n = 11,348) to Zeb1-expressing CGNs
1296 restored migration, suggesting that the GZ exit phenotype Ptch1 deficient GNP is
1297 dependent on Zeb1 repression of its targets. Average migration distance shown in
1298 accompanying graph. Note: the criteria for rescue was set if the condition resulted in cell
1299 distribution that was 80% similar to the Cre Mut distribution (χ^2 -test $p>0.8$) and the
1300 average migration distance was less than 3% similar than the Cre WT condition (t-test
1301 $p<0.03$). Cre Mut vs Cre WT, [χ^2 test] $p(\chi^2) = 2.86 \times 10^{-3}$, [t-test] $p(t) = 3.03 \times 10^{-3}$.
1302 Controls vs Zeb1 shRNA $p(\chi^2) = 0.48$, $p(t) = 0.03$. Controls vs Pard6a $p(\chi^2) = 1.00$, $p(t)$

1303 = 0.01. Controls vs Chl1 $p(\chi^2) = 0.86$, $p(t) = 4.78 \times 10^{-3}$. Controls vs Lin7a $p(\chi^2) = 1.00$,
1304 $p(t) = 1.99 \times 10^{-3}$.

1305 **Supplementary File Legends**

1306 **Supplementary file 1A and 1B:** The results of mouse EMT pathway focused RT²
1307 Profiler™ PCR array. A fold change filtering was performed from three independent
1308 experiments using $2^{-\Delta\Delta Ct}$ (where $\Delta\Delta CT = \Delta CT$ of FACS sorted Zeb1 overexpressing
1309 GNPs– ΔCT of control GNPs) and is represented as tables. The threshold for cut off was
1310 a fold change $\geq +2.0$ or ≤ -2.0 . **Supplementary Table 1A:** Functional gene grouping
1311 shows an upregulation in expression of several genes such as Anhak, Col3A1, Gng11,
1312 MMP2 and3, Serpine (Pals-1) and Vim all of which are documented to be highly
1313 expressed during EMT. **Supplementary Table 1B:** Reciprocal expression of several
1314 key genes that are also downregulated during EMT included Dsp, Fgfbp1, Mst1r.
1315 Additionally Krt14, Nodal and Sox10 genes that are involved in differentiation showed a
1316 reduced expression when Zeb1 was overexpressed.

1317

1318 **Supplementary file 2**

1319 **Supplementary Table 2A:** Neurite length and Ki67 or p27 labeling data from Figure 5.
1320 **Supplementary Table 2B:** Average migration distance and EdU labeling data from
1321 Figure 6

1322

1323 **Supplementary file 3**

1324 **Supplementary Table 3A:** List of primers used for RT-PCR in microarray validation and
1325 developmental profile expression analysis. **Supplementary Table 3B:** Primer

1326 Sequences used for validating the ChIP -PCR studies. **Supplementary Table 3C:** List
1327 of Antibodies.

1328

1329 **Video Descriptions**

1330 **Video 1.** Representative time lapse imaging sequence of a CGN migrating in a
1331 dissociated culture labeled with Centrin2-Venus (green, centrosome) and RFP-UTRCH
1332 ABD (f-actin). The focused cell undergoes typical two-stroke nucleokinesis with f-actin
1333 accumulation in the leading process. Time stamp= hours : minutes : seconds. Scale
1334 bar= 10 μ m.

1335

1336 **Video 2.** Representative time lapse imaging sequence of Zeb1 over-expressing CGNs
1337 migrating in a dissociated culture labeled with Centrin2-Venus (green, centrosome) and
1338 RFP-UTRCH ABD (f-actin). The featured cells undergo random amoeboid movements
1339 with isotropic f-actin decorating the cell periphery. Note the centrosome does not adopt
1340 a polarized configuration as in Video 1. Time stamp= hours : minutes : seconds.
1341 Scale bar=10 μ m.

1342

1343 **Video 3.** Representative time lapse imaging sequence of control CGNs labeled with
1344 Centrin2-Venus (green, centrosome) and H2B-mCherry (nucleus) in a dissociated
1345 culture. The migrating cells in the field undergo typical two-stroke nucleokinesis with
1346 centrosome entering the leading process prior to somal translocation. Note: even
1347 stationary cells extend long neurites. Time stamp= hours : minutes : seconds. Scale
1348 bar= 10 μ m.

1349

1350 **Video 4.** Representative time lapse imaging sequence of Zeb1 over-expressing CGNs
1351 labeled with Centrin2-Venus (green, centrosome) and H2B-mCherry (nucleus) in a
1352 dissociated culture. The migrating cells in the field undergo random amoeboid
1353 movements where the centrosome adopts an unpolarized position in the cell body.
1354 Note: even stationary cells extend do not extend long neurites. Time stamp= hours :
1355 minutes : seconds. Scale bar= 10 μ m.

1356

1357 **Video 5.** Representative time lapse imaging sequence of Zeb1 over-expressing CGNs
1358 with restored Pard6a expression labeled with Centrin2-Venus (green, centrosome) and
1359 H2B-mCherry (nucleus) in a dissociated culture. The migrating cells in the field undergo
1360 typical two-stroke nucleokinesis with centrosome entering the leading process prior to
1361 somal translocation. Note: even stationary cell extend long neurites. Time stamp=
1362 hours : minutes : seconds. Scale bar= 10 μ m.

1363

1364 **Video 6.** Representative time lapse imaging sequence of Zeb1 over-expressing CGNs
1365 with restored Pard3a expression labeled with Centrin2-Venus (green, centrosome) and
1366 H2B-mCherry (nucleus) in a dissociated culture. The migrating cells in the field undergo
1367 typical two-stroke nucleokinesis with centrosome entering the leading process prior to
1368 somal translocation. Note: even stationary cell extend long neurites. Time stamp=
1369 hours : minutes : seconds. Scale bar= 10 μ m.

1370

1371 **Video 7.** Representative time lapse imaging sequence of Zeb1 over-expressing CGNs
1372 with restored Chl1 expression labeled with Centrin2-Venus (green, centrosome) and
1373 H2B-mCherry (nucleus) in a dissociated culture. The migrating cells in the field undergo
1374 typical two-stroke nucleokinesis with centrosome entering the leading process prior to
1375 somal translocation. Note: even stationary cell extend long neurites. Time stamp=

1376 hours : minutes : seconds. Scale bar= 10 μ m.

1377

1378 **Video 8.** Representative time lapse imaging sequence of control CGNs labeled with
1379 JAM-C-pHluorin (green, adhesions) and H2B-mCherry (nucleus) in a dissociated
1380 culture. Note: exuberant cell contacts are observed among most cells. Time stamp=

1381 hours : minutes : seconds. Scale bar= 10 μ m.

1382

1383 **Video 9.** Representative time lapse imaging sequence of Zeb1 over-expressing CGNs
1384 labeled with JAM-C-pHluorin (green, adhesions) and H2B-mCherry (nucleus) in a
1385 dissociated culture. Sparse cell contacts are observed among most cells. Time stamp=

1386 hours : minutes : seconds. Scale bar= 10 μ m.

1387

1388 **Video 10.** Representative time lapse imaging sequence of Zeb1 over-expressing CGNs
1389 with restored Pard6a expression labeled with JAM-C-pHluorin (green, adhesions) and
1390 H2B-mCherry (nucleus) in a dissociated culture. Note: note cell contacts are observed
1391 among most cells. Time stamp= hours : minutes : seconds. Scale bar= 10 μ m.

1392

1393 **Video 11.** Representative time lapse imaging sequence of Zeb1 over-expressing CGNs
1394 with restored Pard3a expression labeled with JAM-C-pHluorin (green, adhesions) and
1395 H2B-mCherry (nucleus) in a dissociated culture. Note: restored cell contacts are
1396 observed among most cells. Time stamp= hours : minutes : seconds. Scale bar= 10
1397 μm.

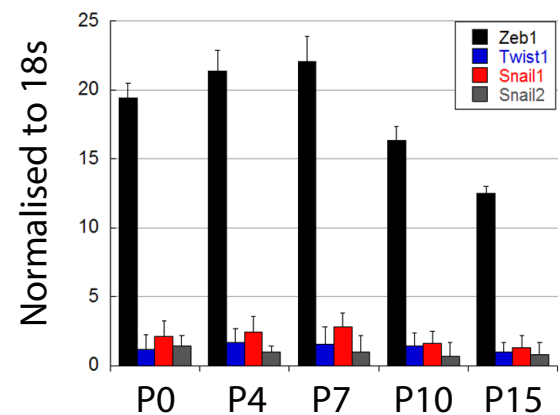
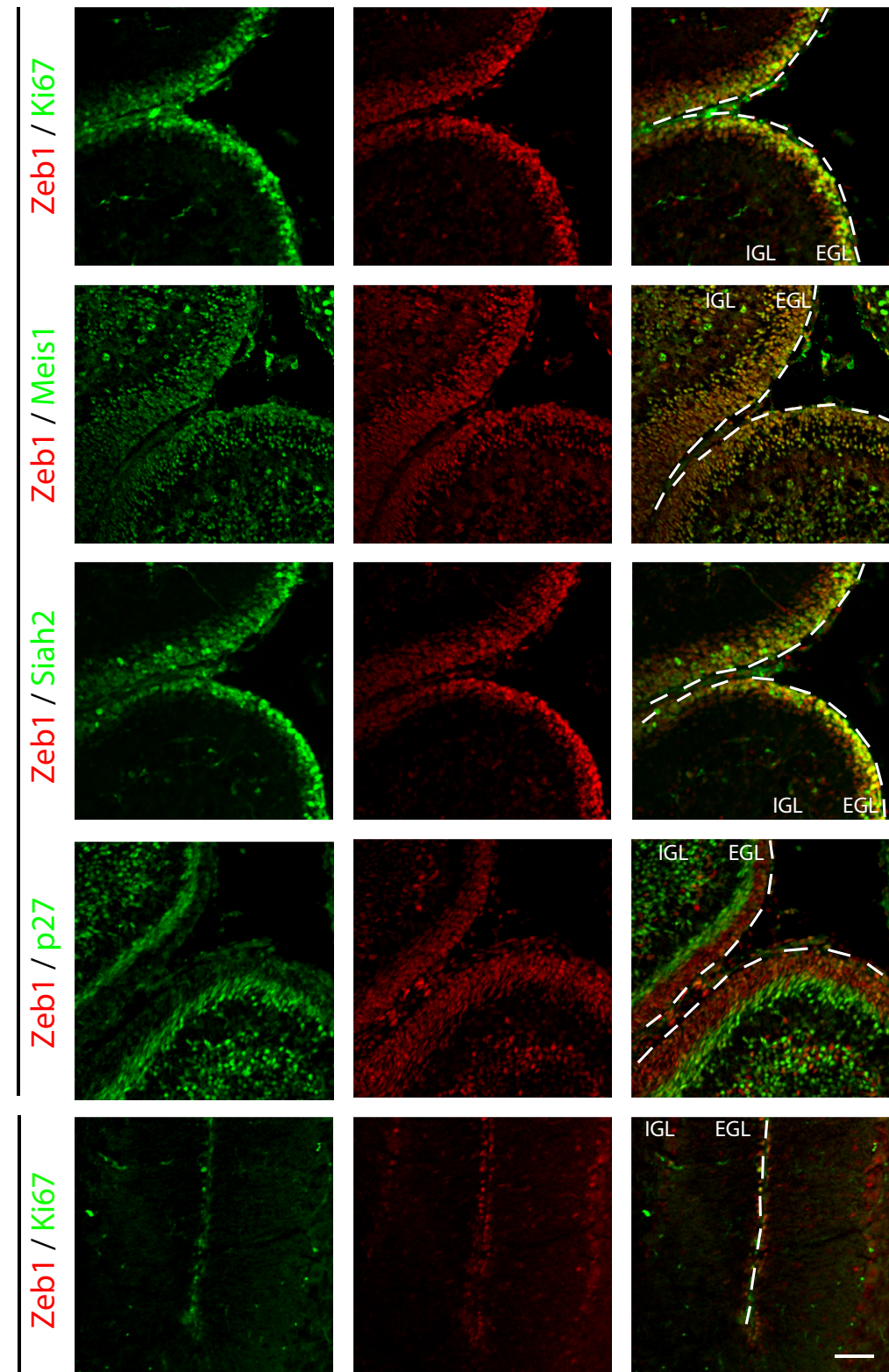
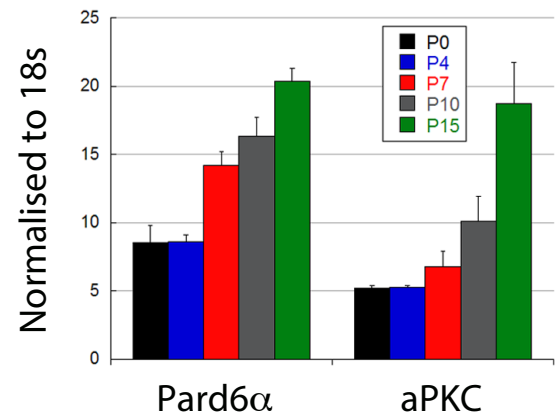
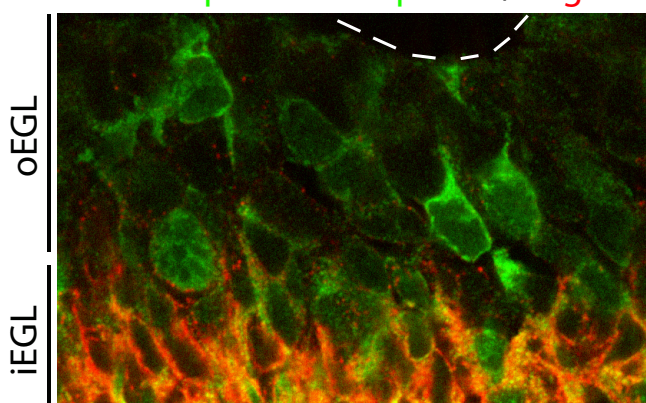
1398

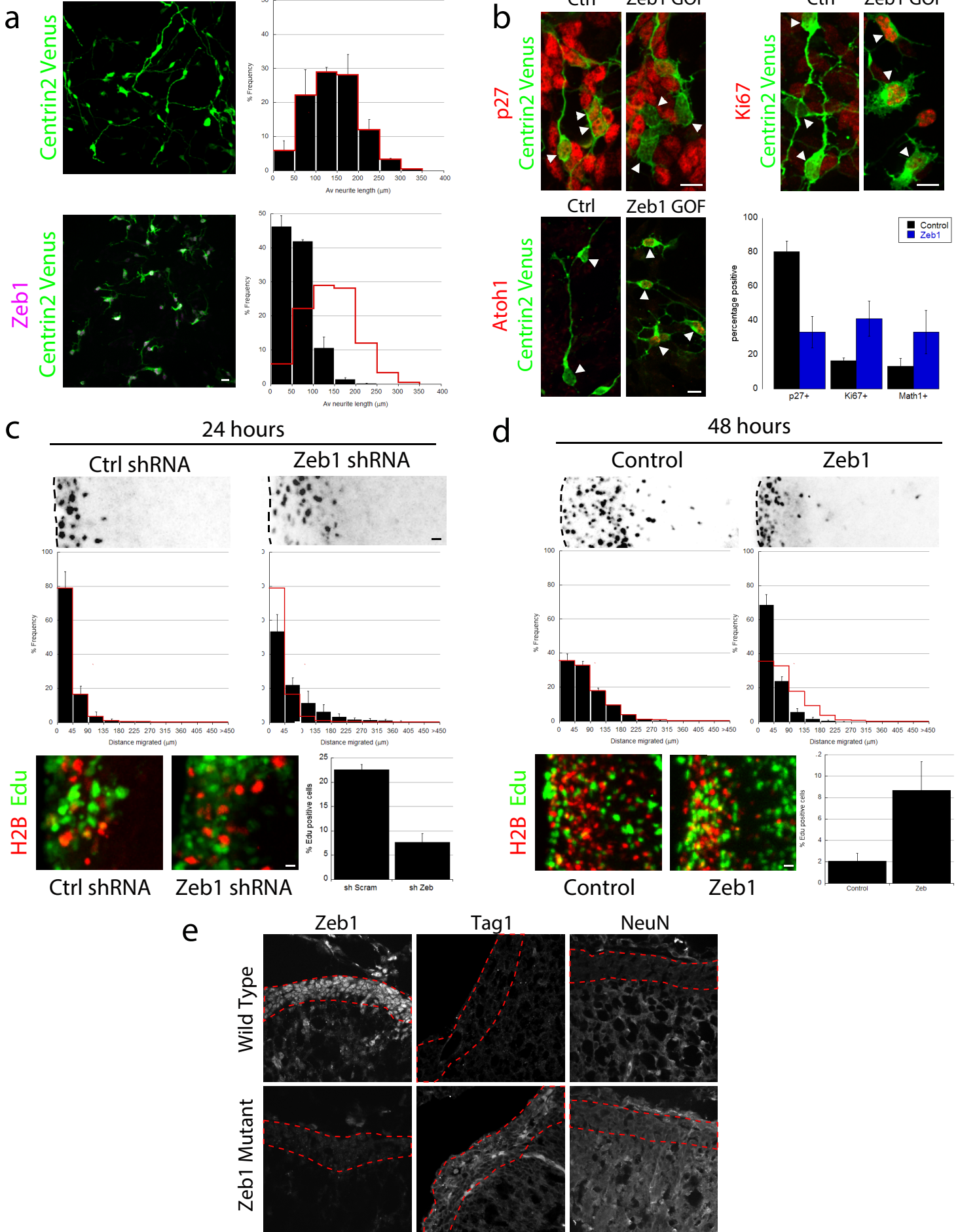
1399 **Video 12.** Representative time lapse imaging sequence of Zeb1 over-expressing CGNs
1400 with restored Chl1 expression labeled with JAM-C-pHluorin (green, adhesions) and
1401 H2B-mCherry (nucleus) in a dissociated culture. Note: restored cell contacts are
1402 observed among most cells. Time stamp= hours : minutes : seconds. Scale bar= 10
1403 μm.

1404

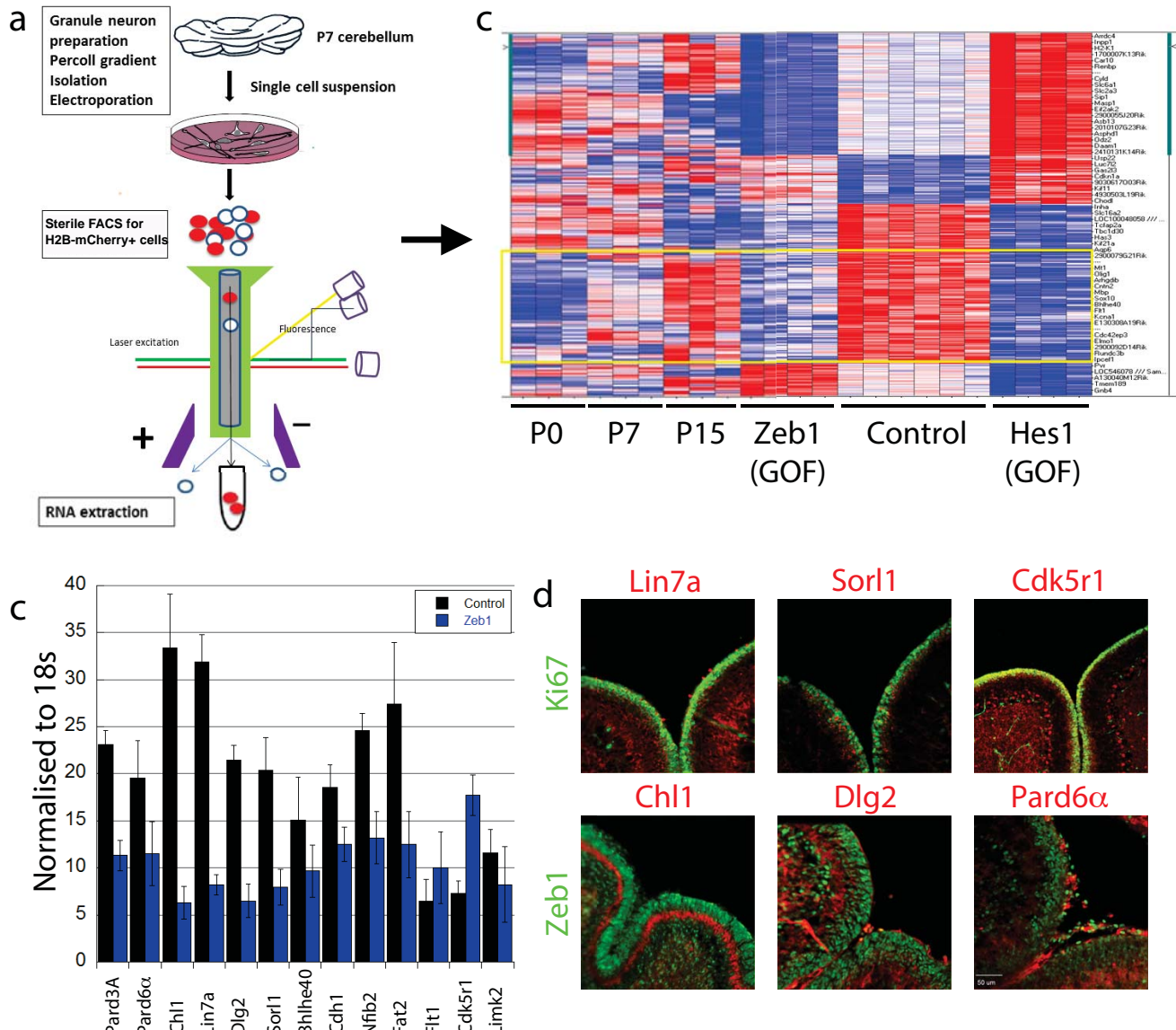
1405

1406

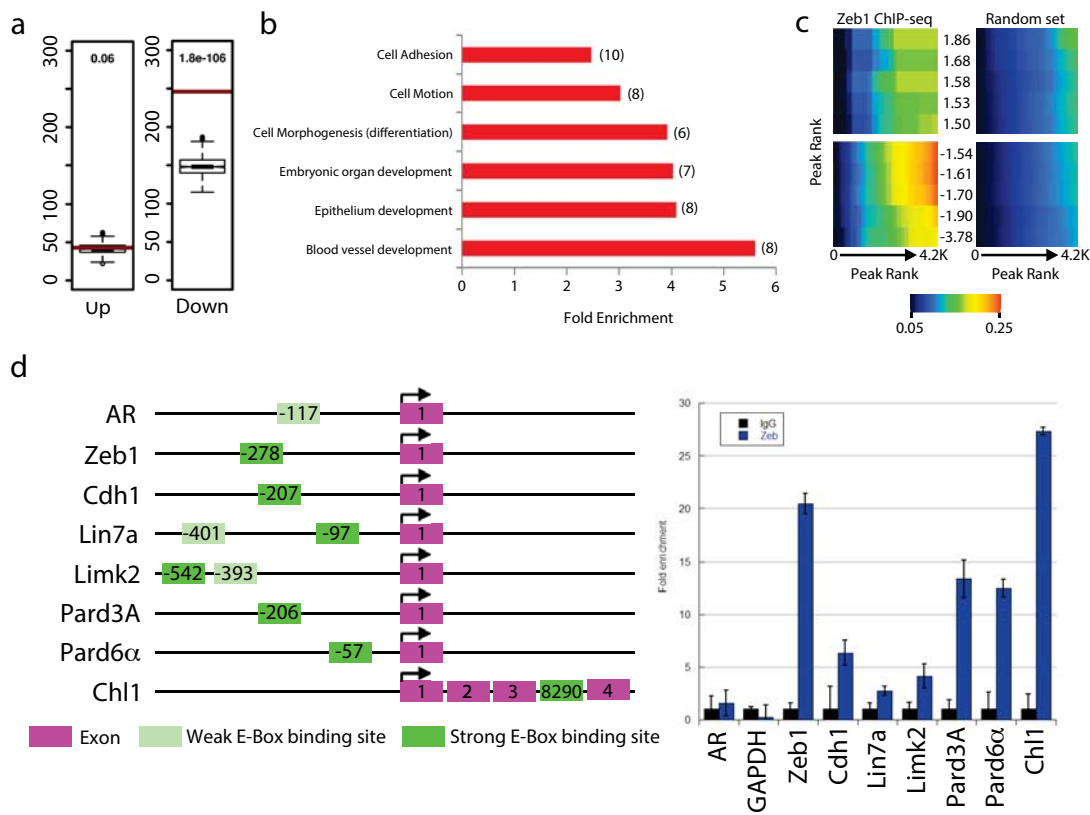
a**b****c****d****Singh et al. Figure 1**



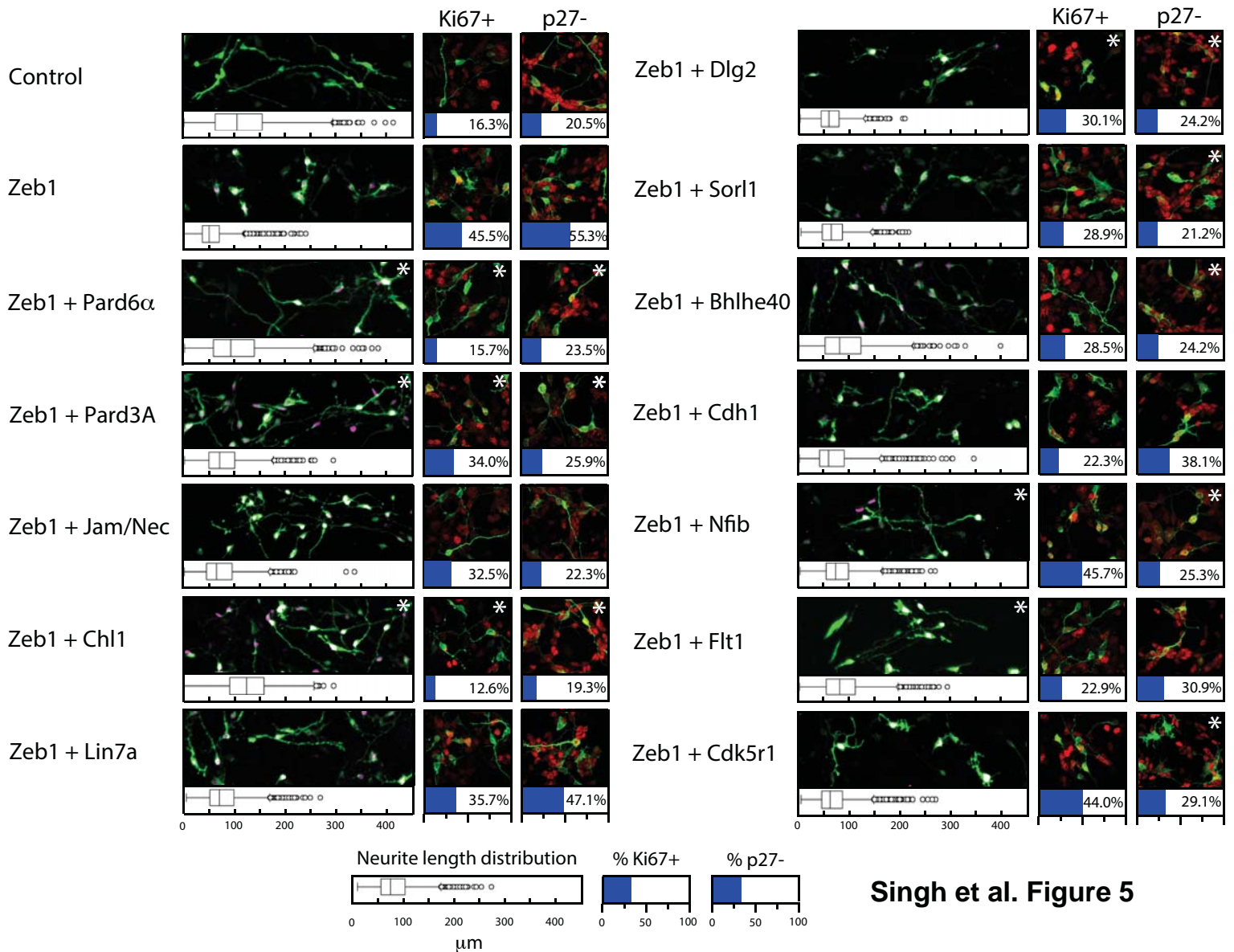
Singh et al. Figure 2



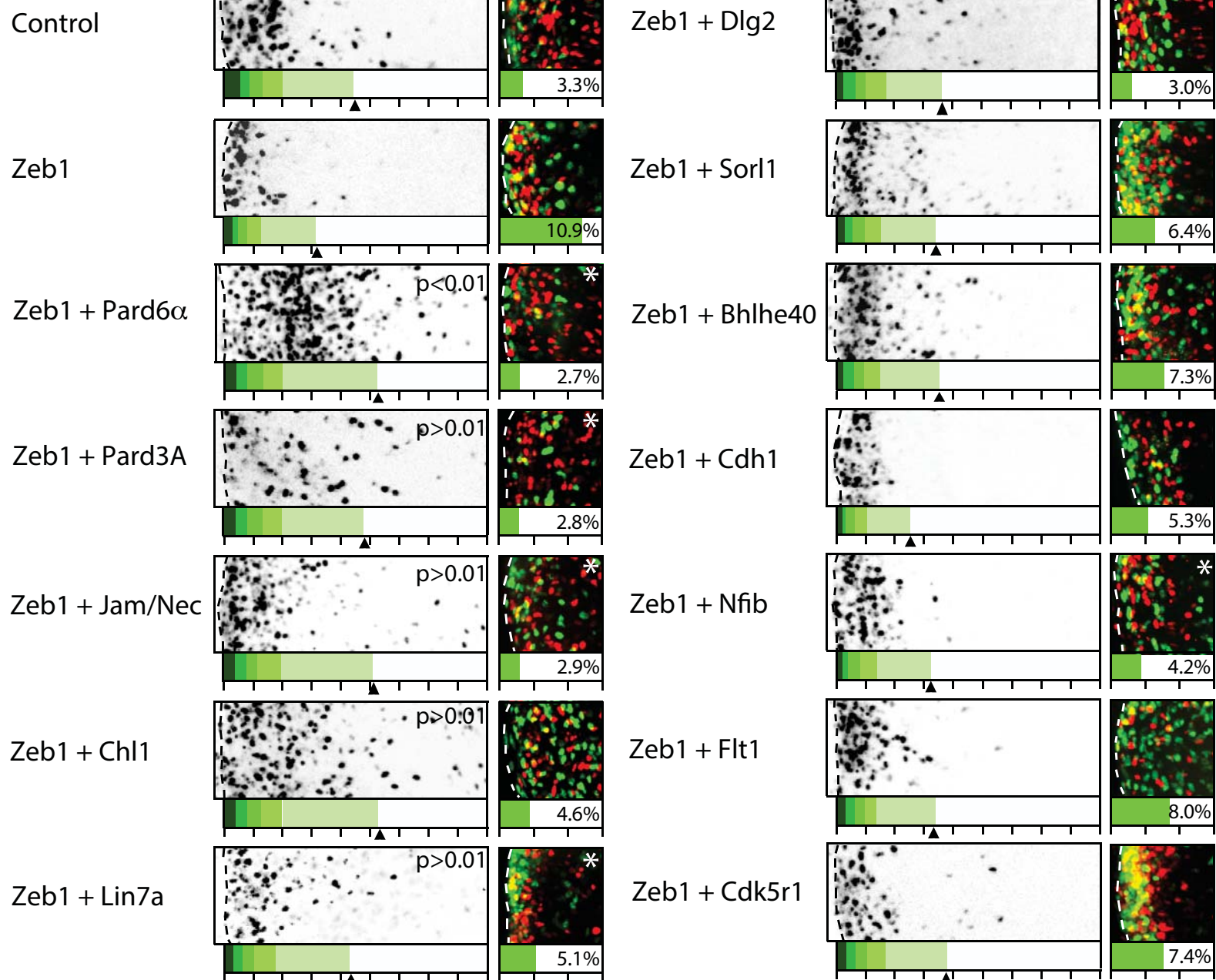
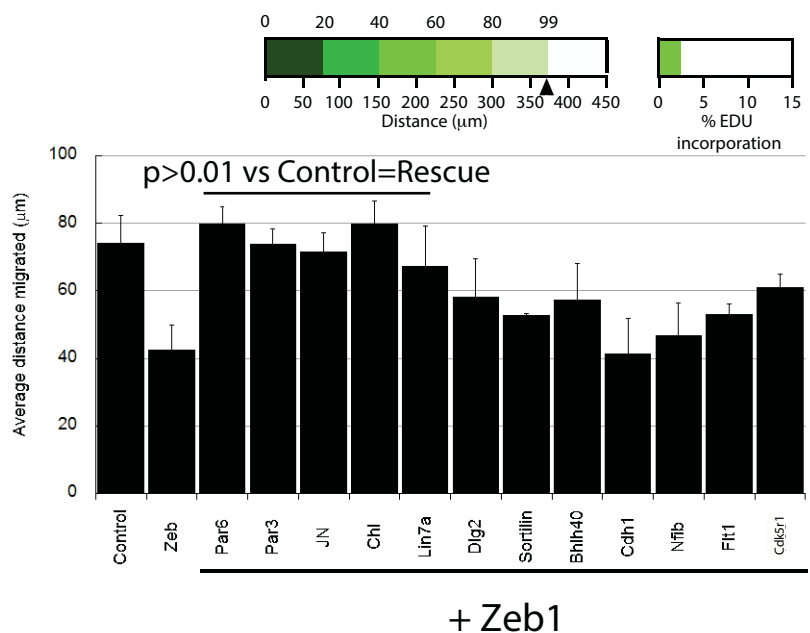
Singh et al. Figure 3

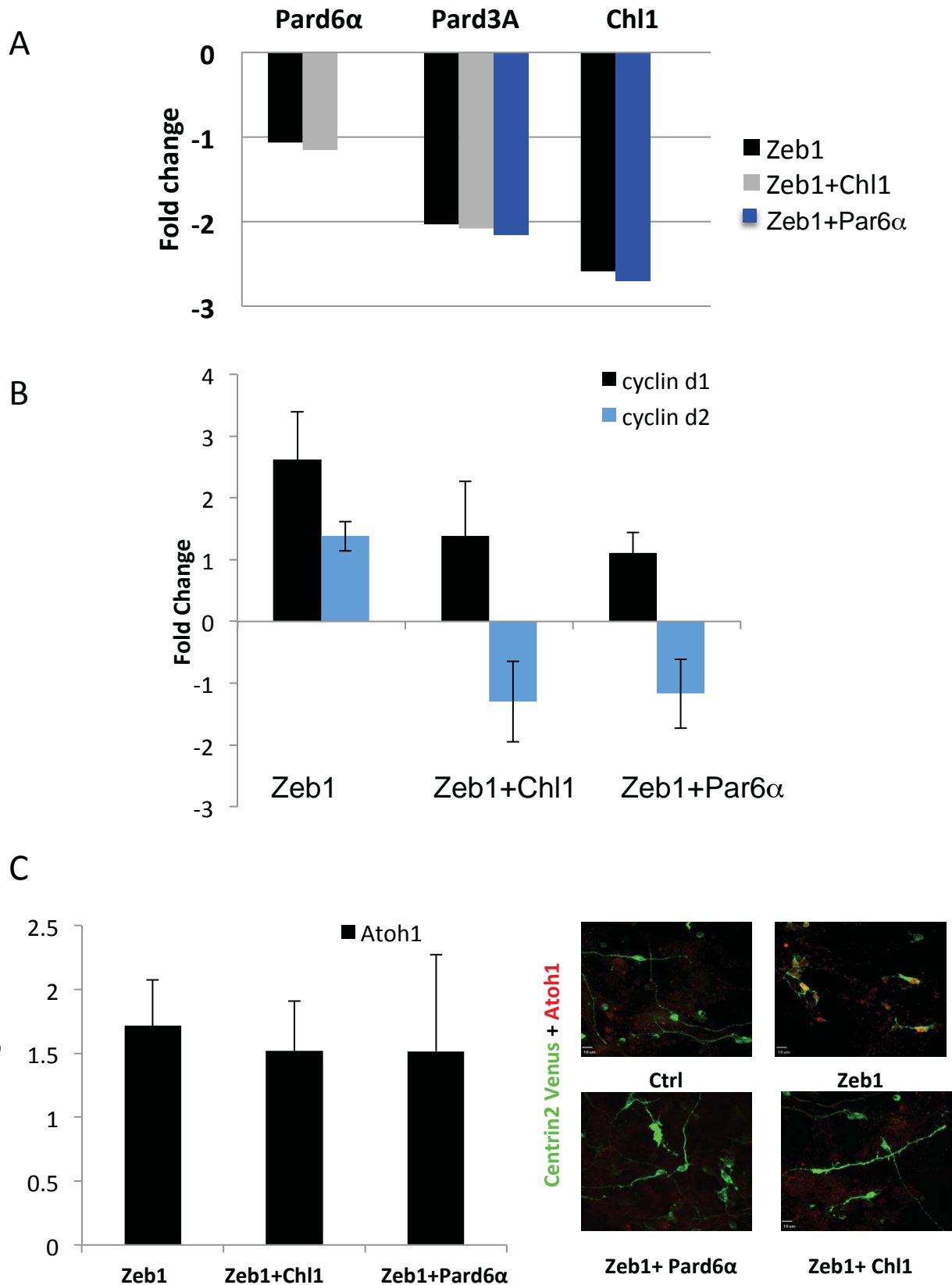


Singh et al. Figure 4

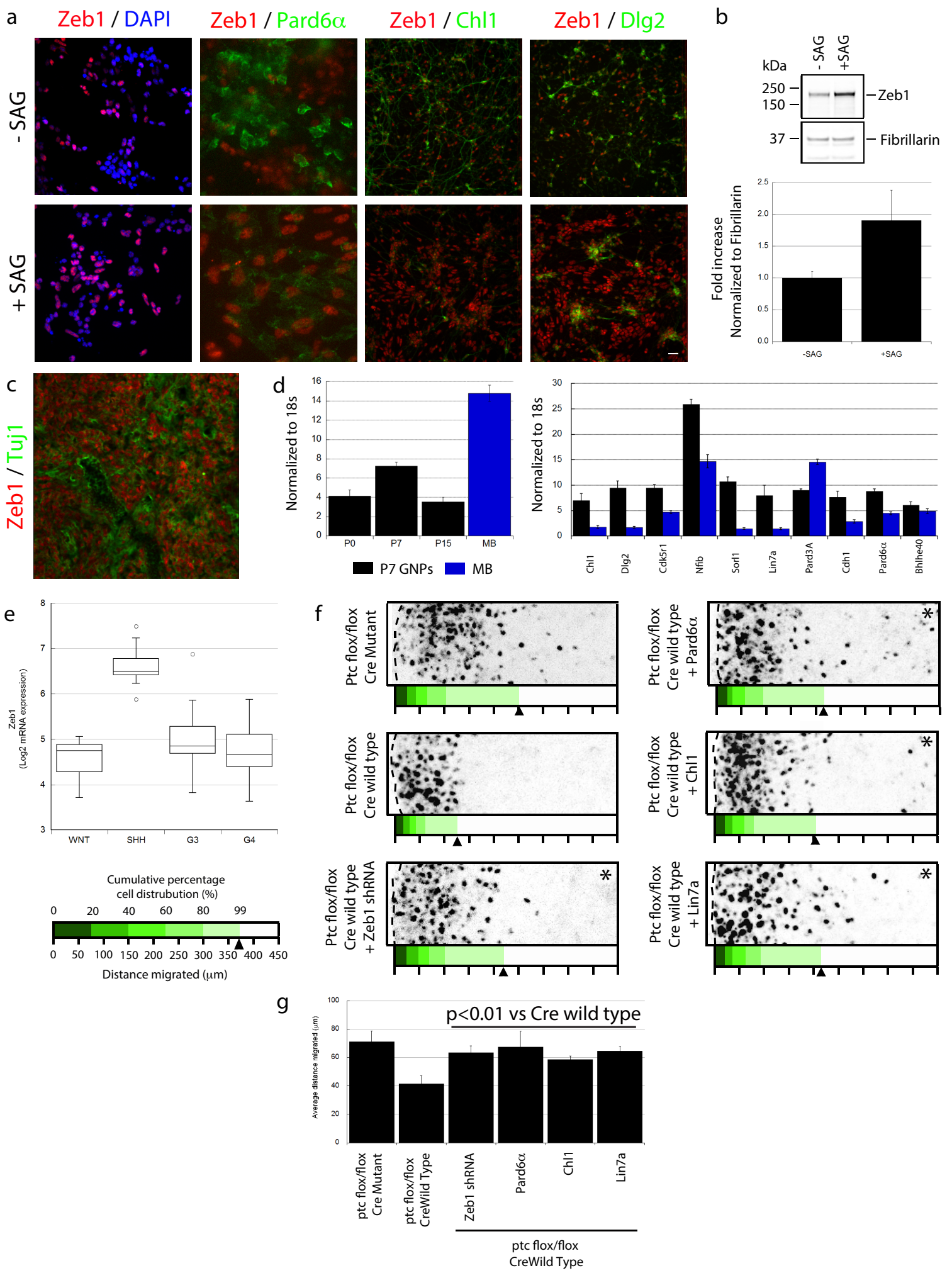


Singh et al. Figure 5

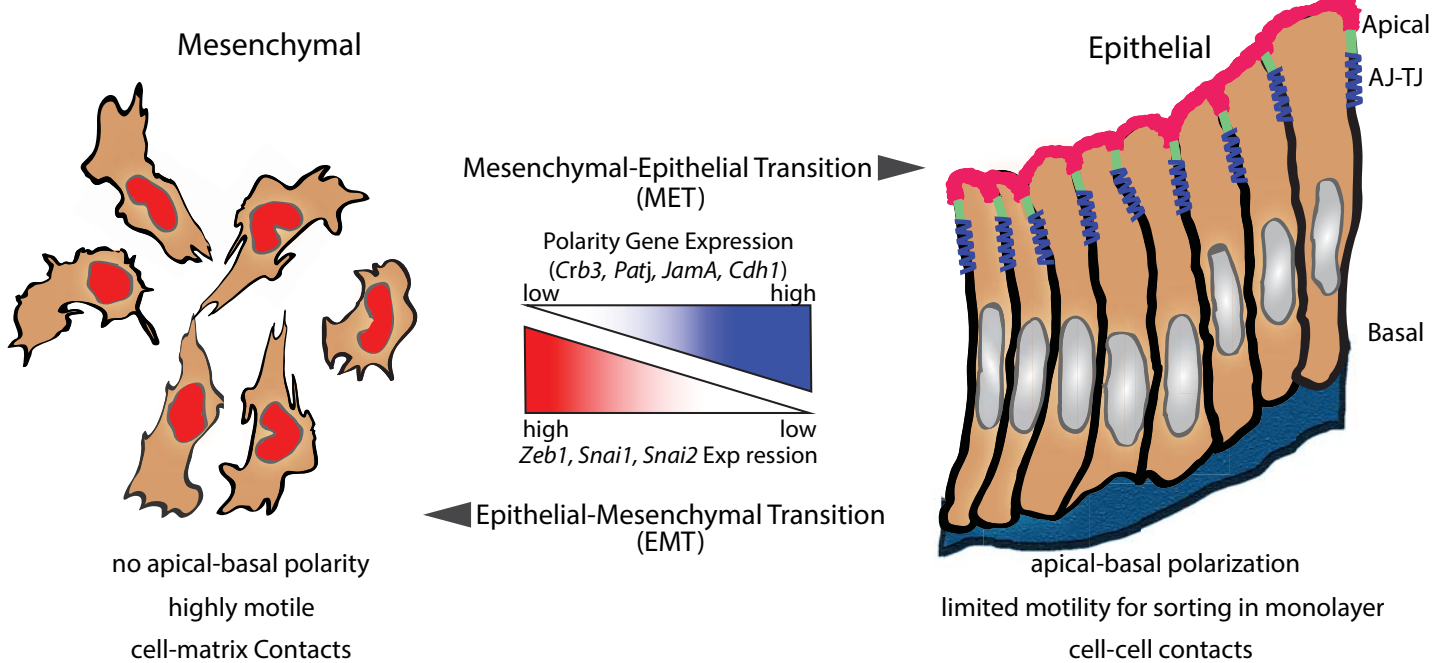
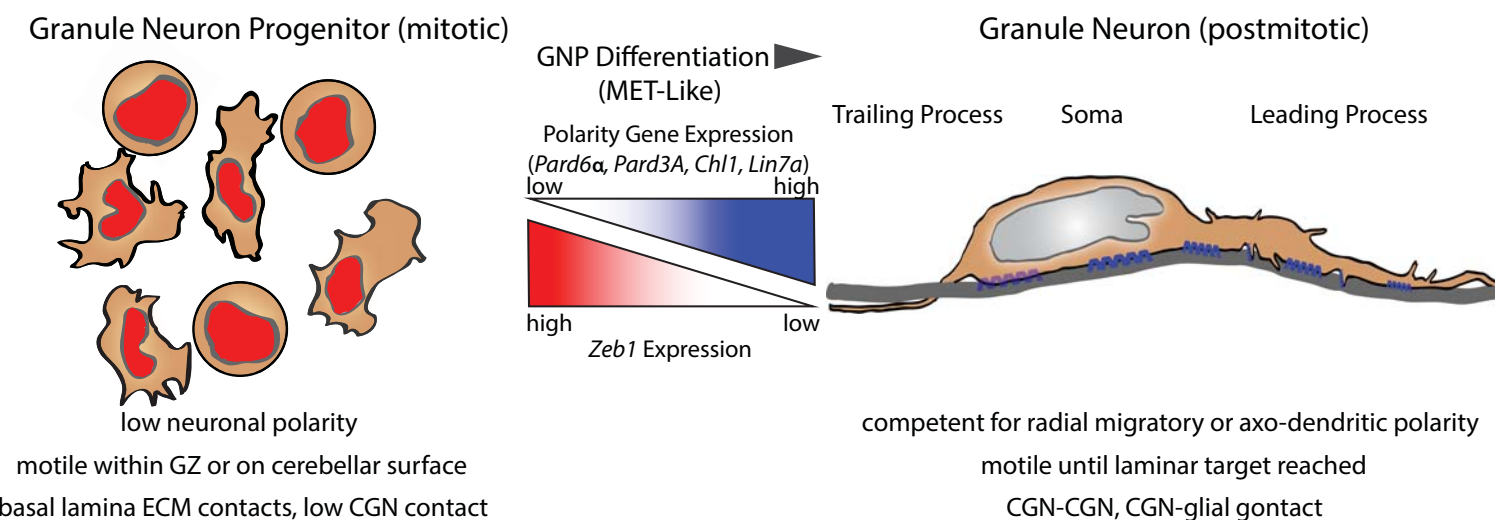
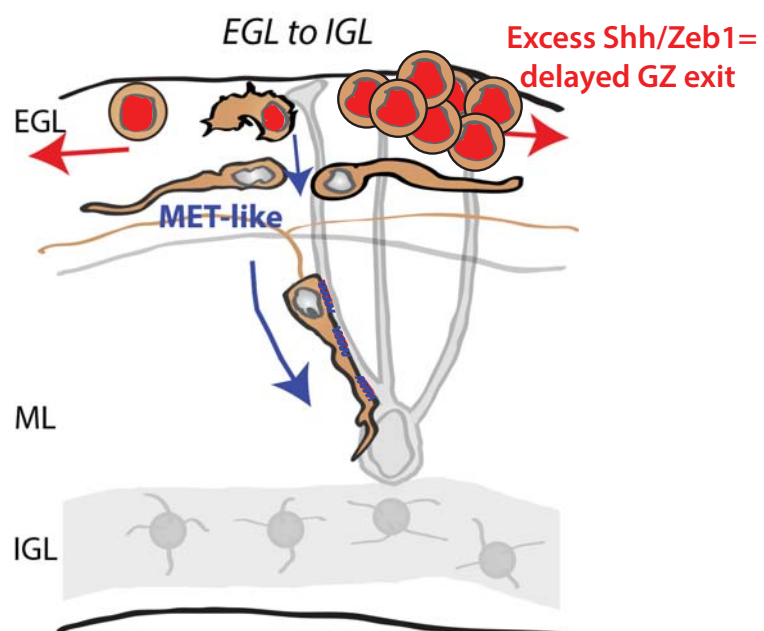
a**b****Singh et al. Figure 6**



Singh et al. Figure 7



Singh et al. Figure 8

a**b****c**

Singh et al. Figure 9